Environ Earth Sci (2015) 74:2571–2593
DOI 10.1007/s12665-015-4277-y

ORIGINAL ARTICLE

Origin of arsenic in Late Pleistocene to Holocene sediments in the Nawalparasi district (Terai, Nepal)

Stéphane Guillot[1] · Marion Garçon[1] · Beth Weinman[2] · Ananta Gajurel[3] · Delphine Tisserand[1] · Christian France-Lanord[4] · Alex van Geen[5] · Sudipta Chakraborty[6] · Pascale Huyghe[1] · Bishal Nath Upreti[3] · Laurent Charlet[1]

Received: 9 July 2014 / Accepted: 5 March 2015 / Published online: 18 March 2015

Abstract A sedimentological and geochemical study was carried out to explore the origin of arsenic contamination in sediments in Nawalparasi district, in the western Terai of Nepal. The investigation tools include major, trace and rare earth element analyses of core sediments, as well as ^{14}C datings, and O, C isotopic analyses on mollusk shells. The results show that black schists from the Lesser Himalaya highly contributed to the detrital input in Parasi during the Pleistocene–Holocene transition because of focused erosion related to rapid uplift and high rainfall along the Main Central Thrust zone. In addition, aquifer silts, sands, and most of the brown clays underwent a certain degree of chemical weathering and physical reworking, and show possible inputs from the Siwaliks during the Late Holocene. A possible correlation between late Quaternary climate regimes and the concentration of arsenic in sediments is suspected, with arsenic preferentially concentrated during the drier periods of the last 25 kyr BP. The process of arsenic eluviations in sandy and silty sediments can explain the lower arsenic concentrations in sediments during humid periods. During the drier periods, seasonal precipitation was smaller and temperature was lower, leading to wet (less evaporative) soils in swampy environments. This environment favoured the development of aquatic plants and bacteria growing within in the moist land areas, enhancing the strong weathering of initially suspended load particles (micas and clays), which were preferentially deposited in quiet hydraulic environments. These sorting and weathering processes presumably allowed the arsenic to be concentrated in the finest sediment fraction.

Keywords Sediments · Geochemistry · Arsenic · Climate · Terai · Nepal

✉ Stéphane Guillot
stephane.guillot@ujf-grenoble.fr

[1] ISTerre, University of Grenoble Alpes, CNRS, 38031 Grenoble, France

[2] Earth and Environmental Sciences, California State University, Fresno, USA

[3] Institute of Science and Technology, Tribhuvan University, Kirtipur, Kathmandu, Nepal

[4] Centre de Recherches Pétrographiques et Géochimiques, CNRS, 54501 Vandoeuvre lès Nancy, France

[5] Lamont-Doherty Earth Observatory of Columbia University, Palisades, New York, USA

[6] Department of Chemistry, Kanchrapara College, Kanchrapara 743145, West Bengal, India

Introduction

Arsenic contamination in groundwater is a growing crisis in parts of South Asia, including Nepal, Bangladesh, India and Pakistan where inhabitants living on alluvial plains of the Himalayan foreland basins depend heavily on groundwater for their daily needs. In this region, arsenic has a geogenic source and its elevated concentrations are considered to be due to natural weathering of the Himalayan belt (Acharyya et al. 2000; Gurung et al. 2005; Guillot and Charlet 2007). In fact, the sediments carried by the Ganga–Brahmaputra river system mainly contributed to the filling of the Himalayan foreland basin and of the Bengal fan, which is considered to be one of the largest modern fluvial deltas of the world (France-Lanord et al. 1993; Garzanti et al. 2004). The amount of sediments carried by the Ganga–Brahmaputra rivers from the Himalayan belt to the delta is estimated at 1800 tonnes/km^2 with suspended loads estimated between 540 and 1175 millions tonnes/year

(Milliman and Sivitsli 1992). The aim of this study is to understand whether the aquifer sediments, having different arsenic concentrations, derived from the same initial source of the Himalaya. The importance of this work defines how pre-depositional processes, such as variable source terrains and/or climate, can affect aquifer deposits and their geochemical variability.

In an attempt to identify how sediment sources and weathering processes can affect local distributions of arsenic, core sediment samples from the Nawalparasi District (Terai, Nepal) were collected by boring and were analysed for major, trace and rare earth elements (REE). In addition, O and C isotopes were performed on mollusk shells that were collected during aquifer sampling. Finally, we contextualize our geochemical findings here to other relevant sedimentological and geochronological works, where we reconstruct the history of the aquifer using our own and other published ^{14}C datings.

Geological setting

Himalayan geology and hydrology of the Terai plain

Extensively exposed in the Narayani basin (Fig. 1) are all four major Himalayan tectonic units: (1) the Tethys Himalaya, delimited at the base by the South Tibetan Detachment system (STDS); (2) the Higher Himalayan Crystallines (HHC) delimited at the base by the Main Central Thrust I (MCT I); (3) the Lesser Himalaya (LH) divided into upper and lower Lesser Himalaya, is delimited at the base by the Main Boundary Thrust (MBT); and (4) the Siwaliks, delimitated at its base by the Main Frontal Thrust (MFT) and the Quaternary foreland basin. These units span a wide range of different metamorphic, sedimentary, and igneous origins, making it possible for their differential erosion to account for some of the groundwater arsenic heterogeneity we see in the foreland and delta (i.e. van Geen et al. 2008; Gurung et al. 2005; Shah 2008). In the region of provenance of the studied basin, the Tethys Himalaya includes 10 km of various metasedimentary rocks (limestones, calc-schists, shales, quartzites) ranging from Cambrian to Jurassic (Colchen et al. 1986). Metamorphism increases upward from amphibolite-facies to anchizonal conditions in the Mesozoic sequence. There is the Manaslu leucogranite emplaced within the Tethyan rocks (Guillot et al. 1995). The Higher Himalayan Crystallines are a metamorphic stack, including from base to top (Colchen et al. 1986) 2–10 km thick paragneisses (metapelites and metapsammites); ~3 km-thick gneisses with calcsilicate minerals (diopside and amphibole) and ~300–500 m-thick orthogneisses representing metamorphosed Lower Paleozoic granites. The Lesser Himalaya consists of mostly unfossiliferous metasediments with a lower part consisting of very low to low-grade quartzites and phyllites (Kuncha Group). The upper part includes some dolomitic meta-carbonates alternating with dominant black schists, aluminium rich schists and quartzites. Amphibolites occur in both of these groupings (Colchen et al. 1986).

The Siwaliks represent the Cenozoic foreland basin of the Himalayan belt with local thickness of 6 km in Nepal (Mugnier et al. 1999; Huyghe et al. 2005). They are divided into three units having a typical coarsening-upward succession. The lower unit consists of fluvial channel sandstones alternating with calcareous paleosols; the middle unit consists of very thick channel sandstones with minor paleosols, and the upper unit mainly hosts conglomerates of gravelly braided river deposits.

The southern plains of Nepal, known as the 'Terai,' are remarkably flat, lie between 60 and 360 m above sea level, and stretch from east to west, in front of the Main Frontal Thrust (Fig. 1). Geologically, the Terai plain is an active foreland basin consisting of Quaternary sediments that include molasse sediments along with gravel, sand, silt and clay. According to a sedimentation rate of 2 mm/year for the recent period, the first 50 m of sediment comprising the shallow aquifers in the region should roughly represent the last ~100,000 years, recording the Late Pleistocene to Holocene periods. Many rivers feeding sediments into the Terai flow south from the Himalayan range (Fig. 1). Minor rivers emanate from the nearby Siwalik Hills and deposit fine and gravelly sediments in the form of a fan system (Shukla and Bora 2009; Upreti 1999). In between the fans, fine sediments and organic material have been depositing in inter-fluvial lowlands in which present-day wetlands and swamps are located (Shah 2008).

Although the Terai constitutes less than 20 % of the Nepal's surface, it contains over half of the total arable land and is home to about 50 % of the total Nepalese population, i.e. 30 millions of inhabitants. Groundwater is the main source of water for drinking and irrigation in the Terai area. Over 90 % of the Terai population draws groundwater from tube wells for drinking, household use, and irrigation (http://www.gwrdb.gov.np/hydrogeological_studies.php). An estimated 800,000 shallow (<20 m) tube wells and over 3000 deep (20–100 m) tube wells exist in the Terai plain (Pokhrel et al. 2009). High monsoon precipitation (2000 mm) and summer snow-fed river systems recharge the Terai sediments giving them high potential for groundwater resources. Shallow aquifers (<50 m) are generally unconfined or semi-confined, whereas the deep aquifers (>50 m) are mostly confined by clay layers (Gurung et al. 2005). Regional groundwater flows southward and the shallow aquifers are highly sensitive to precipitation. However, in the Nawalparasi district, only 10 % of the average rainfall of 2000 mm/year infiltrates and recharges the groundwater systems (UNDP 1989).

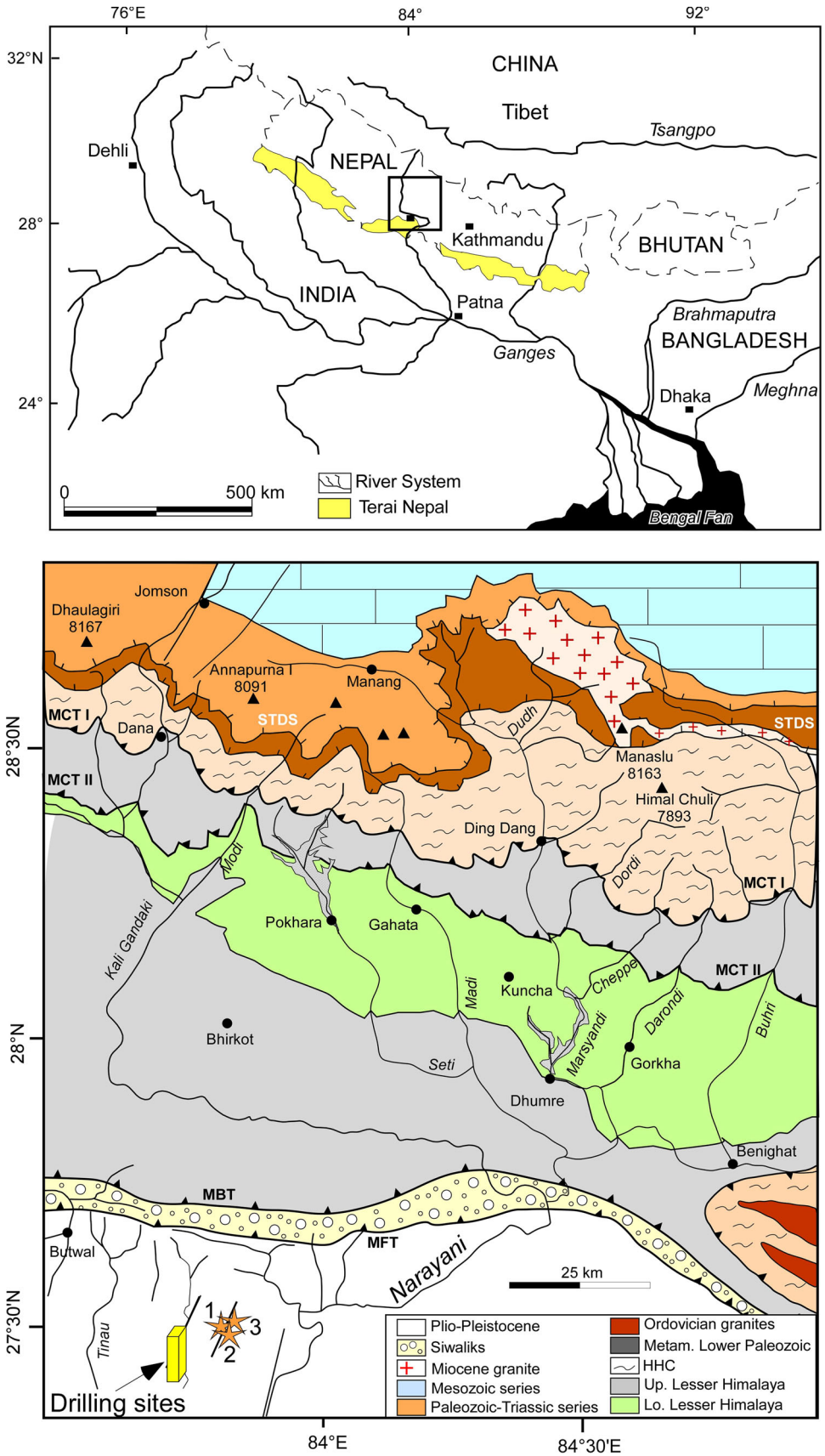

Fig. 1 **a** Location of Terai basin, Nepal, in the Ganga–Brahmaputra watershed areas (after Gurung et al. 2005). **b** Geological map of central Nepal (after Guillot 1999) with the location of drilling sites of this study (*yellow box*) including the three drilling sites studied by Gurung et al. (2005) (*three orange stars*)

Study area and lithology

The study area is located in the Indo-Gangetic plain of the Nawalparasi district in Nepal and comprises the sediments of the inter-alluvial fan deposits between the Narayani and Tinau Rivers (Fig. 1). The area is ~25 km south from the frontal mountain chain of the Himalaya. In between the Tinau and Narayani, small ephemeral rivers originating from the Siwalik frontal mountains disappear upon entering into the Indo-Gangetic plain and reappear again close to the study area. Hence, small natural ponds and river meanderings were observed as characteristic geomorphic features of the area. Close to the frontal mountain chain, the Indo-Gangetic plain consists of boulder- to gravel-sized sediments, while the sediments of the study area are dominantly fine-grained sediments. Five wells were manually drilled down to a depth of about 25 m below ground level (bgl) in the area covering an east–west transect of ~1 km around the Unwach village between 27°31′01″N and 27°30′54″N and 83°39′40″E and 83°40′30″E (Fig. 1b).

Lithology of sledge core samples from the five drill holes shows various coarse (millimetric) to fine-grained (micrometric) sediments. We distinguish light-grey to dark grey sands; grey, greenish-grey to brown-grey and yellow–brown silts; and light-grey to black-grey, yellow–brown and black clay with occasional gravel layers. To facilitate the interpretation of the data, the studied samples have been categorised into three major sediment facies: (1) grey-black clays, (2) brown clays and (3) silts and sands (Table 1). Some calcretes were also observed. Macroscopic observations show that on average, the drilled sediments are composed of 33 % of silts; 30 % of grey to black clays, 27 % of brown clay, 9 % of fine-grained silt and sand and less than 1 % of calcrete. Sands, silt and clay sediments often contained micas that were occasionally massive to laminated, bioturbated, and/or also containing roots and plant debris. Binocular observations show that the detrital minerals in the silt fraction are dominated by quartz, biotite, muscovite, K-feldspar, calcite and dolomite as major phases and garnet, zircon, and monazite as heavy minerals. Abundance of very fine-grained particles is typical of flood plain sediments along the modern Ganga river system including the Narayani river as inferred from present-day deposits (Galy et al. 1999; Singh 2009). The identified sediment facies in Parasi's 25 m shallow subsurface were interpreted as channel, point bar, overbank, and oxbow lake deposits of rivers derived from the Siwalik foothills (Fig. 2).

Muddy sediments with angular to sub-angular gravels appeared at around 24 m depths are interpreted as channel deposit (Fig. 2). Three distinct yellow–brown, brown to yellow–grey paleosol horizons containing calcareous nodules are some of the more obvious and remarkable features in the aquifer. The lowermost, ~3 m thick paleosol at ~21 m depth is extensively distributed in the surveyed area. In studying the wash-borings, we found the paleosols often containing calcareous nodules, or 'kankars', which are principally comprised of microcrystalline calcite with traces of quartz grains (Fig. 2). To compare the lateral extent of our observed facies, we incorporate sedimentological results from other studies, such as the work done by Gurung et al. (2005), located 2–3 km NNE to NE of our study area (Fig. 1b). Inasmuch, data coming from nearby sedimentological environments will be integrated in our discussion, to put into context and better assess the general interest of our findings.

Methods

Major-element data were obtained at the University of Grenoble using a Perkin-Elmer 3000 DV ICP-OES and following a procedure similar to that described by Cotten et al. (1995). The running conditions for the ICP are given in Chauvel et al. (2011) and calibration of the signal is performed using a blank and five different dilutions of a mixed solution of pure elements prepared to mimic the major-element composition of rock samples.

Trace-element concentrations were obtained using an Agilent 7500ce ICP-MS. About 100 mg of rock powder were precisely weighed and dissolved in steel Paar bombs with two rock standards (BIR-1 and UB-N). Dissolution was performed in a mixture of high-purity HF and $HClO_4$ for a minimum of 7 days. After complete dissolution, the solution was evaporated and the residue was treated in concentrated HNO_3 and evaporated before dilution in about 40 mL of 7 $molL^{-1}$ HNO_3. A precisely weighed aliquot of this "mother" solution, corresponding to 8 mg of the starting powder, was mixed with a spike containing five elements (Be, Ge, In, Tm, Bi) and diluted in 2 % HNO_3 with traces of HF to reach a dilution factor of about 5000 (only 2500 for BIR-1 and UB-N). This forms the final solution that is introduced into the ICP-MS.

Measuring the arsenic content of the sedimentary samples requires a specific treatment because the As concentrations of many samples are far higher than those in the standard used to calibrate the ICP-MS signal. We use a doping technique in which a known amount of pure arsenic standard solution is added to an international rock standard final solution before analysis on the ICP-MS. Most elements were measured without using the collision cell (the no-gas mode), but data for eight elements (Sc, Ti, V, Cr, Co, Ni, Cu and Zn) were acquired using a helium flux through the collision cell. A rock standard was used to calibrate the signal and was run every four samples through

Table 1 Geochemical composition in major elements (wt %) of the Nawalparasi borehole sediments and rocks coming from Himalaya (*HHC* higher himalayan crystallines, *LH* lesser himalaya, *Siw* siwaliks)

Samples	Depth	Lithology	SiO_2	TiO_2	Al_2O_3	Fe_2O_3	MnO	MgO	CaO	Na_2O	K_2O	LOI	Total
PNS1	8	Silt	81.08	0.41	8.49	2.82	0.09	0.92	2.79	0.67	2.00	0.20	99.48
PNS1	15	Silt	87.07	0.26	3.87	2.32	0.13	0.38	2.84	bdl	1.10	1.20	99.16
PNS1	15	Brown clay	60.46	0.53	10.95	3.96	0.16	2.02	11.19	0.56	2.78	7.30	99.91
PNS1	18	Brown clay	57.14	0.66	14.10	5.42	0.19	1.94	11.33	1.45	3.30	3.80	99.35
PNS 2/10	3	Brown clay	56.03	0.53	18.04	5.81	0.05	1.88	3.06	0.24	3.97	10.01	99.63
PNS 2/20	6	Brown clay	58.88	0.50	19.49	7.66	0.05	1.45	0.42	0.18	3.96	7.19	99.78
PNS 2/25	8	Silt	95.17	0.22	2.43	1.40	0.04	0.05	0.26	0.00	0.79	0.00	100.36
PNS 2/28	8	Grey clay	61.67	0.47	12.77	4.64	0.06	1.70	5.29	1.29	2.74	8.88	99.51
PNS 2/30	9	Silt	79.01	0.57	8.54	3.49	0.17	1.00	2.04	0.00	2.38	1.20	98.39
PNS 2/35	11	Grey clay	64.74	0.62	12.38	4.67	0.41	2.05	5.41	0.00	3.04	5.30	98.63
PNS 2/36	11	Grey clay	64.04	0.54	12.75	4.78	0.13	1.61	3.62	1.24	2.77	7.65	99.14
PNS 2/39	12	Silt	75.20	0.27	9.40	1.94	0.08	0.63	5.78	1.08	2.27	3.20	99.84
PNS 2/50	15	Calcrete	63.29	0.76	15.33	5.54	0.06	2.42	3.85	1.09	3.87	3.60	99.80
PNS 2/52	16	Brown clay	41.82	0.47	11.96	5.01	0.11	1.74	17.00	1.21	3.03	16.48	98.84
PNS 2/57	17	Silt	68.41	0.39	9.32	2.34	0.06	1.17	7.65	1.68	2.24	5.12	98.37
PNS 2/60	18	Silt	62.56	0.47	11.04	2.94	0.05	1.51	10.53	1.90	2.73	6.15	99.88
PNS 2/62	19	Grey clay	51.64	0.55	19.34	6.79	0.22	2.48	2.74	0.34	4.22	10.98	99.30
PNS 2/63	19	Grey clay	53.31	0.54	18.15	7.00	0.03	2.43	0.85	0.58	4.01	12.43	99.33
PNS 2/67	20	Black clay	56.42	0.54	18.04	6.06	0.05	2.32	1.81	0.47	3.89	9.84	99.44
PNS 2/69	21	Brown clay	58.41	0.67	14.91	5.40	0.08	2.55	7.03	0.00	3.21	6.70	98.95
PNS 2/75	23	Brown clay	49.16	0.53	14.85	5.39	0.10	1.96	10.17	0.26	3.24	12.80	98.47
PNS 2/80	24	Black clay	63.35	0.87	18.07	5.50	0.07	2.89	1.32	0.00	4.51	3.10	99.68
PNS 3/5	2	Silt	78.85	0.50	7.75	3.39	0.11	0.90	1.48	bdl	2.20	4.50	99.70
PNS 3/10	3	Brown clay	69.58	0.57	13.51	4.46	0.04	1.20	0.22	0.44	3.21	5.85	99.07
PNS 3/15	5	Silt	74.29	0.70	11.99	4.70	0.11	1.25	0.37	bdl	3.15	2.70	99.27
PNS 3/18	5	Brown clay	66.11	0.44	14.64	6.19	0.04	1.22	0.24	0.42	3.09	6.57	98.96
PNS 3/28	8	Grey clay	63.40	0.59	17.45	5.48	0.04	1.88	0.38	0.47	4.11	4.73	98.53
PNS 3/32	10	Grey clay	52.55	0.62	21.14	6.35	0.03	2.33	0.73	0.22	4.33	11.06	99.37
PNS 3/37	11	Grey clay	58.20	0.52	16.08	6.02	0.13	2.65	3.03	0.55	3.83	8.47	99.48
PNS 3/40	12	Silt	71.71	0.30	9.90	2.17	0.05	1.14	4.25	1.84	2.22	3.85	97.43
PNS 3/45	14	Brown clay	58.05	0.51	11.31	3.98	0.10	2.05	12.55	0.86	2.69	7.40	99.50
PNS 3/46	14	Grey clay	43.79	0.47	11.90	4.72	0.08	1.93	16.43	1.36	3.15	15.15	98.97
PNS 3/47	14	Brown clay	62.79	0.70	14.40	4.46	0.08	2.23	6.83	1.23	3.59	3.30	99.61
PNS 3/55	17	Silt	62.26	0.43	11.87	3.21	0.05	1.54	7.73	1.95	3.26	6.05	98.34
PNS 3/60	18	Silt	71.05	0.42	9.25	2.57	0.04	1.22	6.01	1.49	2.54	4.53	99.12
PNS 3/62	19	Grey clay	62.65	0.48	15.41	5.51	0.03	1.69	0.62	0.62	3.53	7.80	98.34
PNS 3/70	21	Brown clay	77.95	0.43	8.87	3.10	0.05	0.84	0.48	0.59	2.08	3.91	98.31
PNS 3/85	26	Grey clay	69.28	0.51	12.82	3.73	0.03	1.35	1.01	0.50	2.96	5.70	97.87
PNS 4/5	2	Grey clay	66.19	0.87	17.47	5.76	0.08	2.26	0.48	bdl	4.31	2.20	99.62
PNS 4/12	4	Grey clay	58.39	1.11	17.81	6.94	0.14	1.08	4.83	4.13	3.12	2.30	99.85
PNS 4/17	5	Brown clay	70.72	0.56	13.37	4.28	0.03	1.23	0.23	0.52	3.27	4.57	98.78
PNS 4/35	11	Black clay	59.56	0.52	15.19	5.30	0.04	1.87	1.20	1.00	3.37	10.45	98.51
PNS 4/45	14	Brown clay	47.48	0.48	12.55	4.63	0.08	2.08	13.62	1.56	3.24	13.38	99.10
PNS 4/53	16	Silt	68.61	0.46	9.27	2.71	0.04	1.32	7.33	1.43	2.50	5.04	98.71
PNS 4/60	18	Brown clay	71.41	0.39	9.24	3.67	0.07	1.02	2.83	0.44	2.13	6.70	97.90
PNS 4/63	19	Silt	75.61	0.54	9.35	3.92	0.11	1.13	2.80	bdl	2.27	3.10	98.84
PNS 4/67	20	Grey clay	61.83	0.83	16.57	6.85	0.02	3.42	2.03	bdl	3.53	4.60	99.68
PNS 4/69	21	Grey clay	61.24	0.54	15.21	6.05	0.03	1.61	0.88	0.67	3.68	9.49	99.40

Table 1 continued

Samples	Depth	Lithology	SiO_2	TiO_2	Al_2O_3	Fe_2O_3	MnO	MgO	CaO	Na_2O	K_2O	LOI	Total
PNS 4/72	22	Silt	73.40	0.53	9.55	4.40	0.26	1.15	4.31	0.16	2.27	3.70	99.74
PNS 4/74	22	Grey clay	50.00	0.45	16.73	6.67	0.07	2.43	5.58	0.49	3.50	13.29	99.21
PNS 5/10	3	Silt	77.73	0.61	10.58	4.40	0.07	1.18	0.53	bdl	2.77	2.40	100.28
PNS 5/16	5	Brown clay	71.94	0.28	10.92	4.16	0.06	1.00	1.17	0.50	2.72	5.93	98.68
PNS 5/19	6	Brown clay	82.06	0.41	7.56	2.79	0.02	0.69	bdl	0.44	1.97	2.65	98.58
PNS 5/25	8	Silt	93.42	0.18	2.18	1.01	0.01	0.22	bdl	0.12	0.74	0.74	98.62
PNS 5/30	9	Silt	87.70	0.31	3.62	2.05	0.12	0.32	2.53	bdl	1.20	2.00	99.86
PNS 5/33	10	Silt	94.60	0.28	2.04	1.57	0.00	0.08	0.50	bdl	0.77	0.10	99.95
PNS 5/35	11	Brown clay	68.75	0.28	3.87	3.14	0.34	0.46	14.88	bdl	1.16	6.90	99.79
PNS 5/36	11	Silt	71.00	0.11	3.35	2.26	0.11	0.42	10.77	0.19	0.91	9.78	98.89
PNS 5/40	12	Black clay	55.07	0.55	14.96	6.16	0.05	2.04	2.82	0.89	3.34	13.56	99.43
PNS 5/42	13	Calcrete	45.78	0.28	8.02	2.89	0.14	2.58	23.66	0.74	1.88	14.20	100.14
PNS 5/45	14	Silt	71.22	0.34	8.12	2.25	0.05	0.93	5.93	1.20	1.99	6.38	98.40
TE11	HHC	Gneiss	63.79	0.82	17.25	6.52	0.02	5.08	0.28	2.58	3.01	1.17	100.64
TE12	HHC	Gneiss	68.72	0.74	14.27	5.60	0.04	5.02	0.74	1.72	2.51	1.41	100.89
TE13	HHC	Marble	67.59	0.63	15.59	4.42	0.05	3.30	0.84	4.38	1.62	1.34	99.79
TE19	HHC	Gneiss	76.56	0.63	10.69	4.27	0.05	1.71	0.76	1.27	2.96	1.25	100.29
TE20	HHC	Gneiss	74.20	0.61	10.48	4.71	0.24	1.53	6.34	0.92	0.49	0.72	100.43
TE21	HHC	Calc-gneiss	51.55	0.33	9.00	3.39	0.05	7.42	9.99	0.64	3.10	13.86	99.43
TE23	HHC	Calc-gneiss	38.85	0.33	9.08	3.50	0.07	10.81	13.34	0.13	3.28	21.37	100.86
TE24	HHC	Amphibolite	67.68	0.52	13.35	3.20	0.02	2.90	0.72	1.03	3.27	8.24	100.97
TE26a	HHC	Quartzite	69.20	0.55	15.12	2.37	0.01	2.86	0.75	0.55	4.64	3.82	100.45
TE26b	HHC	Gneiss	47.56	0.33	8.73	1.36	0.04	9.35	10.65	1.18	2.52	17.91	99.76
TE27	HHC	Amphibolite	49.18	1.54	14.48	10.91	0.18	6.84	8.32	4.76	0.08	4.45	100.92
TE28	HHC	Schist	56.61	1.44	11.72	13.21	0.14	6.09	5.07	3.77	0.85	1.84	100.92
TE29	HHC	Quartzite	95.83	0.04	0.81	0.96	0.00	0.71	0.04	bdl	bdl	0.67	99.06
TE10	**LH**	**Black schist**	69.99	0.51	15.28	3.35	0.01	1.42	0.06	1.28	4.18	3.61	99.79
TE2	**LH**	**Black schist**	62.59	0.55	18.14	5.81	0.03	2.62	0.14	0.73	5.16	4.76	100.64
TE30	**LH**	**Black schist**	58.11	0.61	21.88	5.72	0.07	2.03	0.40	1.41	5.88	3.19	99.43
TE35	**LH**	**Black schist**	80.43	0.24	7.94	3.97	0.01	2.20	0.16	bdl	2.78	2.18	100.01
TE1	LH	Marble	11.57	0.02	0.42	1.51	0.08	18.35	26.88	bdl	0.14	41.49	100.48
TE18	LH	Schist	69.11	0.48	14.76	4.85	0.02	2.51	0.36	2.12	4.44	1.94	100.70
TE3	LH	Marble	0.93	0.01	0.24	0.15	0.00	0.30	54.85	bdl	0.07	43.29	99.84
TE31	LH	Serpentinite	45.75	1.86	15.97	10.05	0.15	15.48	1.54	1.96	bdl	6.84	99.76
TE32	LH	Marble	7.49	0.04	0.99	0.72	0.07	19.40	27.80	bdl	0.31	42.34	99.22
TE33	LH	Calc-schist	58.95	0.01	0.20	0.16	0.01	9.07	12.50	bdl	0.06	17.99	98.94
TE34	LH	Calc-schist	54.16	0.41	10.79	4.18	0.06	6.39	7.32	0.20	4.21	12.94	100.75
TE36	LH	Marble	10.26	0.10	2.58	1.02	0.06	19.08	25.94	bdl	1.07	40.48	100.61
TE37	LH	Schist	71.05	0.70	14.07	5.55	0.05	0.96	0.13	0.65	2.84	4.40	100.42
TE38	LH	Schist	88.40	0.54	4.33	3.86	0.01	0.21	0.05	bdl	0.76	2.19	100.41
TE39	LH	Schist	60.08	0.59	19.17	7.27	0.03	1.94	0.03	bdl	5.60	5.43	100.25
TE4	LH	Marble	25.69	0.01	0.26	0.18	0.03	16.12	22.86	bdl	0.07	34.16	99.40
TE40	LH	Schist	78.47	1.43	6.00	7.27	0.16	0.57	1.70	bdl	0.56	3.14	99.50
TE48	LH	Marble	2.67	0.01	0.21	0.17	0.00	21.27	30.06	bdl	0.05	44.94	99.39
TE50	LH	Schist	40.36	0.77	12.60	9.50	0.38	2.21	15.33	0.20	2.35	16.01	99.92
TE7	LH	Marble	19.20		0.07	0.20	0.02	17.72	25.04	bdl	bdl	37.12	99.38
TE8	LH	Dolomite	0.60	0.01	0.53	1.06	0.11	21.21	30.30	bdl	0.07	45.73	99.61
TE9a	LH	Schist	64.85	0.62	17.45	6.11	0.04	2.88	0.41	0.73	3.53	3.48	100.16

Table 1 continued

Samples	Depth	Lithology	SiO_2	TiO_2	Al_2O_3	Fe_2O_3	MnO	MgO	CaO	Na_2O	K_2O	LOI	Total
TE9b	LH	Calc-schist	40.52	0.02	0.47	0.26	0.05	12.77	17.76	bdl	0.16	27.33	99.37
TE41	SIW	Calcrete	35.82	0.31	6.13	4.22	0.15	2.46	25.48	0.30	1.50	23.83	100.28
TE42	SIW	Grey clay	76.94	0.43	6.91	2.33	0.03	1.54	3.96	0.66	1.61	5.40	99.90
TE44	SIW	Calcrete	39.69	0.43	9.48	3.94	0.11	2.79	20.50	0.31	2.84	20.11	100.32
TE45	SIW	Calcrete	44.87	0.48	9.88	3.83	0.13	3.48	16.62	0.57	2.65	17.87	100.50
TE47	SIW	Silt	80.84	0.38	5.85	2.49	0.03	0.85	2.81	0.45	1.62	3.60	98.97

Black schists from the upper Lesser Himalaya are in bold

the entire sequence. In addition, at the start of each daily sequence, pure solutions of Ba, Ce, Pr and Nd were run to evaluate and correct oxide interferences on the middle and heavy REE and the interference of double-charged Nd on Ge. All calculations to transform peak signals into concentrations were done offline. For each element, the average peak signal of the chosen rock standard was used as the calibrating value for all calculations. Before calculation of the element concentrations, we perform three corrections: (1) an oxide interference correction based on the oxide/metal ratio determined with the pure element solutions, (2) a machine drift correction based on the five-element spike with a mass-based interpolation and (3) a blank subtraction. To perform the machine drift correction for both modes (with or without helium), the beryllium and germanium peaks are measured in both modes whereas other spikes are measured only in the no-gas mode. The overall quality of the chemical procedure is controlled as follows: (1) systematic evaluation of the difference between the procedural blank and the running solution blank, (2) the entire chemical and analytical procedure is checked by systematically duplicating at least one sample per batch, and (3) the machine stability is controlled using multiple runs of randomly selected rock solutions.

Shells of freshwater mollusks were found in the clay, silty-clay/clayey-silt, and the fine sand facies (mollusk fossils in Fig. 2). The individual shells were analysed for stable isotopes (C and O) in the laboratory of Centre de Recherche Pétrographiques et Géochimiques, Nancy, France. The mollusk shells were cleaned in distilled water with ultrasound to remove adhered sediments and organic debris. Then, they were reacted under vacuum with $\approx$100 % phosphoric acid at 25 $\pm$ 0.1 °C (McCrea 1950). Isotopic analyses of the released CO_2 were performed in a modified mass spectrometer, model VG 602. Carbon and oxygen isotopic ratios of aragonite are expressed as $\delta^{13}C_{Ara}$ and $\delta^{18}O_{Ara}$ relative to Pee Dee Belemnite (PDB). Following common practice for aragonite shell analyses (e.g. Dettman et al. 1999; Lécuyer et al. 2004), we did not apply any correction specific for aragonite and used the standard correction for calcite. Ten to fifteen repeated analyses of calcite international standards over the analytical period are: NBS-18 ($\delta^{13}C = -5.02 \pm 0.04$ ‰ and $\delta^{18}O = -23.06 \pm 0.13$ ‰), NBS-19 ($\delta^{13}C = 2.00 \pm 0.04$ ‰ and $\delta^{18}O = -2.15 \pm 0.13$ ‰), IAEA-CO-1 ($\delta^{13}C = 2.47 \pm 0.04$ ‰ and $\delta^{18}O = -2.46 \pm 0.09$ ‰), IAEA-CO-8 ($t\delta^{13}C = -5.74 \pm 0.07$ ‰ and $\delta^{18}O = -22.79 \pm 0.1$ ‰). Overall reproducibility is ±0.1 ‰.

Sediment depositional ages were determined when possible by ^{14}C on organic matter (Table 2). Retrieved sediment samples were typically organic-poor, with rare small pieces of preserved terrestrial detritus and shell fragments seen perhaps once in each drill hole. One sample of woody fragments from 7.3 m depth from the last drill hole (Site 5) was retrieved from Nepal and rinsed with distilled water, dried overnight at 60 °C (to 3.5540 g) and sent to Daniel Weinand at the University of Tennessee's Center for Archaeometry and Geochronology (UTAG) for liquid scintillation counting ^{14}C dating.

Results

^{14}C Ages

The wood fragment from $\sim$7 m depth in borehole 5 gives a ^{14}C age between 3354 and 2928 year BC using an average delta-13C value of −26.5 for the fractionation correction (UTAG sample ID 07-013).The final calibrated age was determined using IntCal04/OxCal4.0 for reservoir correction.

Geochemistry

Average geochemical compositions (major and trace elements) of 61 sediments of the Nawalparasi boreholes are reported in Table 2. We also report, when available, the composition of the potential sources using 41 rock samples collected from the Higher Himalayan Crystallines (HHC), the Lesser Himalaya s.l. (LH), the black schists from the Lesser Himalaya and the Siwaliks (Siw) along the Kali

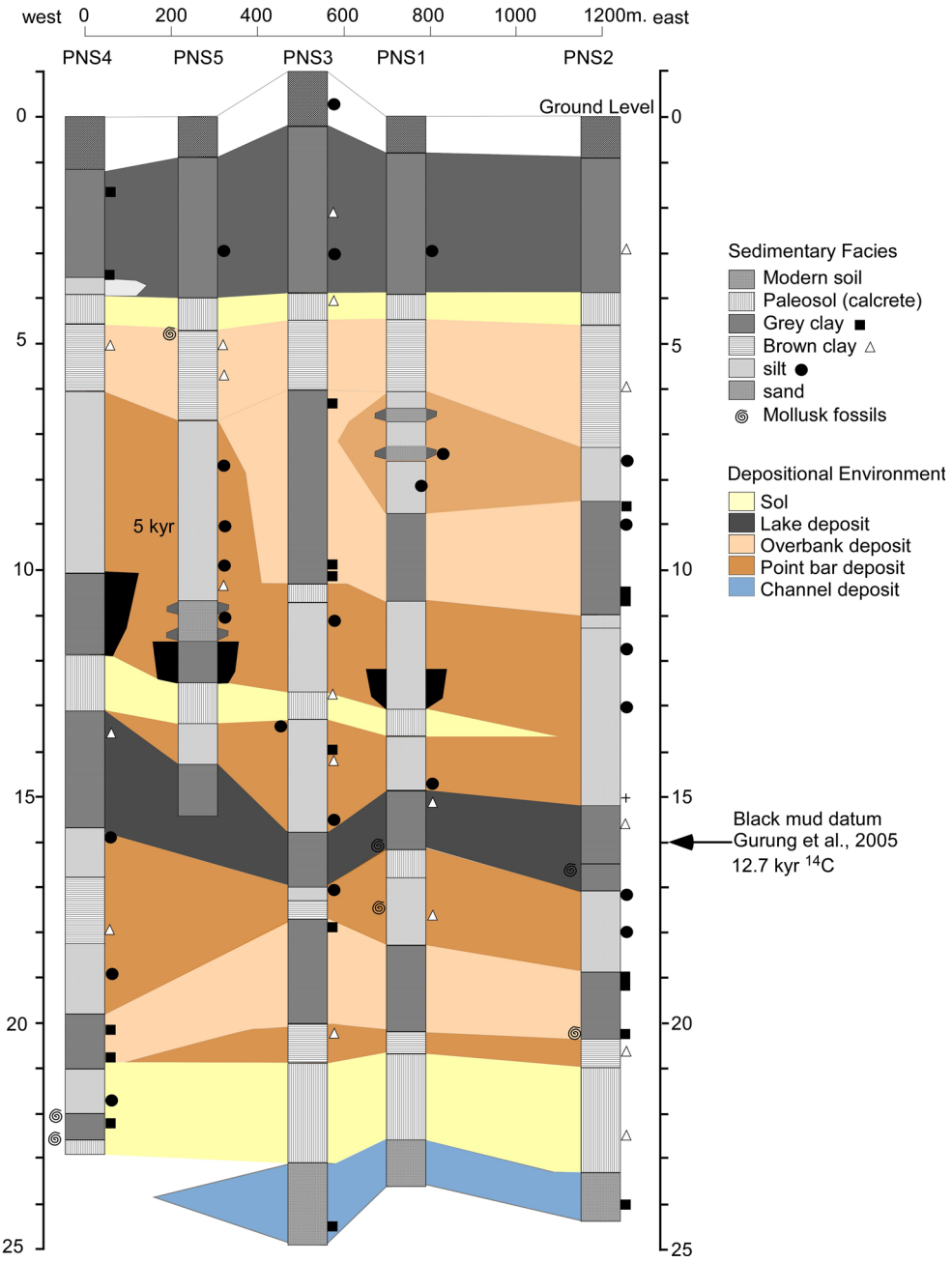

Fig. 2 Interpreted stratigraphic logs of the five drilling bores with sampling depth and OSL ages and ^{14}C dating*

Gandaki, Seti and Narayani rivers (Tables 1, 2). Systematically, the silt and sand fractions are enriched in SiO_2 (between 60 and 90 %wt) relative to the clay fractions (between 40 and 70 %wt). Less mobile elements such as Al_2O_3, Fe_2O_3, MgO, TiO_2 are systematically enriched in the clay fractions for a given SiO_2 content (Fig. 3). Nevertheless, the general negative trend between those elements and the SiO_2 content is partly due to a dilution effect by quartz in the silt and sand fractions. It is noticeable that the grey clays are the most enriched in immobile elements. Na_2O and MnO have similar patterns, depleted in the clay fraction (Fig. 3), and this may be related to a leaching effect in anoxic conditions where Mn(IV) is reduced to Mn(II). Calcium is mostly concentrated in the brown clays and associated with calcrete.

Altogether, 38 samples from the boreholes and 41 samples from the Himalaya were analysed for REEs (Table 3). As before, they were also categorised into the same three sediment-type groupings: grey clay, brown clay, silt-sand. All the groupings of sediments have similar chondrite-normalised REE patterns (Fig. 4) with overlapping abundances. The average REE concentrations show an increase from sand/silt fraction to clay fraction. On average, REE concentrations in the sands and silts are ~30 %

Table 2 Geochemical composition in trace elements of the Nawalparasi borehole sediments and rocks coming from Himalaya (*HHC* higher himalayan crystallines, *LH* lesser himalaya, *Siw* siwaliks)

Samples	As (ppm)	Ce (ppm)	Co (ppm)	Cr (ppm)	Cs (ppm)	Cu (ppm)	Ni (ppm)	Pb (ppm)	Rb (ppm)	Sr (ppm)	Th (ppm)	U (ppm)	Zr (ppm)	C org (%)
PNS 2/10	8.41	101	16	92	12.2	28.8	40.3	34.3	213	45.4	22.8	3.47	164	0.14
PNS 2/20	15	99.9	16.9	99.8	12.4	29.4	42.7	32.6	199	39.7	22.9	3.59	178	0.06
PNS 2/28	17.2	65.6	12.9	77.2	8.65	22.8	37.5	21.2	134	124	14.3	3.81	240	0.41
PNS 2/36	10.2	78	13.3	81.1	8.85	24.8	37.8	24.3	148	108	16.5	3.83	216	0.34
PNS 2/49	3.09	76.5	5.11	30.4	4.9	5.79	10.6	20.6	96.9	183	16.6	3.04	215	0.05
PNS 2/52	3.97	49.9	10.4	53.6	9.24	27.2	28	23.2	139	210	11.8	2.08	100	0.15
PNS 2/57	3.04	81.5	6.16	41.5	4.53	10.2	25.5	20.7	106	241	19.1	3.42	297	0.03
PNS 2/60	2.85	69.8	6.63	38.5	5.82	7.62	14.7	20.4	124	311	16.3	3.39	204	0.04
PNS 2/62	9.87	97	17.5	104	13.8	35	48	32.4	231	86.7	23.4	3.83	132	0.51
PNS 2/63	16.8	87.5	16.8	102	13.7	37	49.4	29.2	216	101	20.4	3.51	144	0.78
PNS 2/67	12.3	86.5	15.8	97.7	11.9	45.3	46.4	29.1	221	107	21.4	3.48	170	0.47
PNS 2/75	10.1	88.7	13.5	77.2	9.96	23.1	32.1	31.8	176	87.9	18.7	3.41	153	0.04
PNS 3/10	7.38	95.7	11.9	69.9	7.89	23.7	27.7	27.1	160	37.9	19.1	3.18	277	0.04
PNS 3/18	10.4	91.9	15	81	9.26	24.2	35.5	26.8	170	38.7	19.8	3.46	242	0.11
PNS 3/28	4.92	107	15.7	93.6	11.5	28.5	40.3	32.9	206	48.3	22.4	3.22	209	0.15
PNS 3/32	6.55	105	18.6	114	14.6	40.2	55.9	35.3	233	54.9	25.4	4.13	143	0.98
PNS 3/37	10.6	93.3	15.1	96.4	9.4	33.2	46	21.7	169	56.2	20.3	3.73	223	1.08
PNS 3/40	2.15	67.3	4.96	32.4	5.64	6.53	11.9	21.7	115	186	14.8	2.6	177	0.05
PNS 3/46	4.17	62	11.8	62.1	11.1	29.5	29.4	24.9	180	277	14.3	2.81	133	0.16
PNS 3/55	2.6	57.1	8.41	51.6	8.34	10.8	21.2	25.1	171	280	12.5	2.42	219	0.09
PNS 3/60	3.27	53.4	6.33	38.5	6.1	8.19	15.1	19.1	127	222	11.6	2.43	289	0.07
PNS 3/62	13.4	90.5	12.6	88.4	10.3	27.6	38.1	25	170	72.9	19.4	5.12	274	0.55
PNS 3/70	6.55	89.4	8.78	50.6	4.88	13.4	23.2	16.4	102	41.3	17.2	3.27	489	0.05
PNS 3/85	4.43	86.6	10.9	68.1	8.3	20.3	29.5	21	158	51.2	18.1	2.73	266	0.15
PNS 4/17	5.86	97.9	10.4	71.1	7.69	19.8	27.3	24.1	158	39.7	19.1	3.28	299	0.15
PNS 4/35	10.8	85.5	12.9	112	10.6	39.9	44.1	23.7	162	90.8	17.8	7.02	195	1.86
PNS 4/45	3.8	74.8	11.7	60.9	10.4	34.4	30.5	25.3	173	271	15.6	3.05	179	0.16
PNS 4/53	3.22	56	7.47	43.7	6.42	6.78	17.1	18.1	129	245	12.4	2.47	215	0.05
PNS 4/60	11.9	77.9	11.2	58.7	5.88	18.4	27.6	20.6	117	71	15.8	3.41	333	0.08
PNS 4/69	27.7	88.9	14	93.4	11.3	31	43.6	26	190	88	19.4	8.06	206	0.73
PNS 4/74	8.56	86.1	16.9	98.7	11.3	34.4	47.6	28.3	190	127	19.2	2.87	138	0.45
PNS 5/16	8.11	78.8	10.3	55.8	6.24	18.5	23.7	23.2	129	35	15.7	2.56	242	0.04
PNS 5/19	3.53	68.8	7.2	39.1	3.94	13	16.9	18.7	87.7	26.1	13.8	2.79	418	0.05
PNS 5/25	1.74	31.5	2.59	14.9	1.32	3.79	5.63	6.95	32.2	10.7	6.03	1.38	283	0.05
PNS 5/36	9.92	76.5	13	78.4	8.73	24.4	37.5	24	145	108	16.2	3.79	217	0.03
PNS 5/40	11	78.5	14.8	112	10.6	49.5	49.2	26.8	171	86.8	17.5	6.04	176	2.73
PNS 5/42	14.5	48.3	10.9	44.7	7.15	20.8	27.6	20.5	107	304	10.7	5.22	130	0.11
PNS 5/45	5.06	60.3	6.09	32.4	5.24	9.37	13.5	19.4	101	134	12.6	2.63	257	0.10
TE11	0.00	5.11	bdl	4.87	2.30	1.50	129.50	bdl	7.04	16.71	128.60	25.76	175.00	nd
TE12	0.00	7.01	12.82	4.78	2.99	1.32	109.60	bdl	18.56	16.23	124.20	26.57	231.30	nd
TE13	0.00	5.99	11.65	3.99	2.14	1.18	71.43	bdl	9.49	14.63	80.01	20.86	187.70	nd
TE19	0.00	4.41	13.16	4.81	2.67	1.21	117.40	bdl	3.31	14.70	69.65	26.58	306.60	nd
TE20	3.15	1.13	bdl	5.93	3.32	1.54	25.61	0.42	5.64	13.19	82.69	35.87	243.20	nd
TE21	0.00	4.78	13.89	3.21	1.83	0.86	124.10	bdl	2.38	10.76	50.97	18.40	134.70	nd
TE23	0.00	4.03	bdl	3.44	1.92	0.81	122.60	0.24	3.12	12.12	46.59	19.99	120.60	nd
TE24	0.00	11.75	24.24	3.44	1.78	1.11	151.20	0.97	2.24	12.65	127.00	18.94	115.90	nd
TE26a	0.00	9.27	7.28	5.59	3.43	1.29	193.90	0.50	3.72	18.68	168.80	37.07	170.40	nd

Table 2 continued

Samples	As (ppm)	Ce (ppm)	Co (ppm)	Cr (ppm)	Cs (ppm)	Cu (ppm)	Ni (ppm)	Pb (ppm)	Rb (ppm)	Sr (ppm)	Th (ppm)	U (ppm)	Zr (ppm)	C org (%)
TE26b	0.00	4.47	71.53	1.67	0.96	0.35	112.80	0.71	2.57	10.49	43.71	9.62	130.00	nd
TE27	2.23	bdl	171.50	4.03	2.13	1.46	0.48	1.80	1.34	3.32	245.60	21.69	130.90	nd
TE28	0.00	7.11	26.71	3.85	2.01	1.40	38.01	0.84	1.49	3.72	292.10	20.37	128.50	nd
TE29	0.00	bdl	bdl	0.39	0.21	0.19	0.33	0.31	0.48	2.00	4.43	2.14	54.36	nd
TE10	18.32	6.54	52.21	3.74	2.49	0.86	168.60	1.13	3.41	14.88	79.63	24.91	187.80	nd
TE2	18.21	11.99	10.55	4.50	2.57	1.27	276.80	1.32	5.01	17.78	99.09	26.73	138.00	nd
TE30	14.01	10.16	6.32	5.68	3.04	1.64	289.20	0.27	7.65	20.28	81.44	31.35	139.80	nd
TE35	17.60	3.04	4.06	3.16	1.67	0.60	92.21	1.35	2.04	8.40	23.43	17.33	142.20	nd
TE1	6.75	bdl	14.76	0.44	0.22	0.16	4.56	0.54	bdl	0.51	13.17	2.79	8.25	nd
TE18	0.00	7.79	bdl	4.31	2.34	1.37	223.40	1.06	3.68	27.71	39.56	24.98	260.20	nd
TE3	0.00	0.19	bdl	0.07	0.05	0.02	3.72	bdl	bdl	0.19	1.27	0.62	2.05	nd
TE31	0.00	0.11	bdl	4.25	2.22	1.76	0.84	1.22	1.25	3.18	272.40	22.80	135.00	nd
TE32	1.85	0.33	bdl	0.72	0.41	0.15	7.61	0.26	0.25	1.75	6.86	4.27	26.80	nd
TE33	0.00	bdl	bdl	0.06	0.03	0.01	1.77	bdl	bdl	0.18	bdl	bdl	2.03	nd
TE34	3.64	9.73	bdl	3.93	2.31	0.93	157.10	1.59	2.93	13.73	49.35	23.24	176.00	nd
TE36	0.00	1.49	bdl	1.58	0.78	0.50	42.29	0.71	0.75	3.04	18.86	9.70	33.45	nd
TE37	7.85	7.44	25.64	6.67	3.67	1.69	131.80	0.43	3.64	17.43	79.83	39.12	276.70	nd
TE38	14.67	1.51	17.07	8.55	3.30	3.32	32.64	1.75	1.19	6.30	43.19	34.77	186.50	nd
TE39	5.94	15.16	27.85	6.02	3.50	1.32	262.10	2.23	5.24	21.03	95.91	36.07	158.20	nd
TE4	3.57	bdl	bdl	0.16	0.10	0.03	2.06	0.24	bdl	0.30	1.80	0.96	2.81	nd
E40	1.90	1.76	25.05	8.73	4.37	2.28	33.00	0.39	2.14	16.02	99.06	45.82	511.30	nd
TE48	0.00	0.25	bdl	0.18	0.10	0.04	2.47	bdl	bdl	0.38	1.65	1.10	5.68	nd
TE50	5.86	4.50	27.70	4.22	2.26	1.28	121.10	0.23	2.31	10.77	110.80	22.75	153.10	nd
TE7	0.00	bdl	bdl	0.07	0.07	0.01	0.54	bdl	bdl	1.72	2.04	0.50	5.23	nd
TE8	0.00	0.14	bdl	0.28	0.15	0.08	3.20	1.08	bdl	0.70	5.18	1.65	3.79	nd
TE9a	0.00	8.80	51.13	4.89	2.58	1.30	196.20	0.20	bdl	18.53	55.71	27.07	136.60	nd
TE9b	5.73	0.11	bdl	0.16	0.09	0.04	4.91	2.17	bdl	0.44	2.97	0.86	4.05	nd
TE41	7.17	3.62	10.42	3.09	1.72	0.75	63.58	1.32	1.84	8.69	38.28	20.04	130.10	nd
TE42	0.00	2.36	14.59	3.49	1.91	0.85	62.19	0.68	1.70	11.73	36.45	19.38	254.30	nd
TE44	10.33	6.18	16.66	4.04	2.22	1.00	123.30	1.36	2.74	12.76	56.62	23.90	106.70	nd
TE45	8.79	5.39	18.61	4.28	2.40	1.05	116.90	1.52	2.82	14.34	59.13	24.87	164.20	nd
TE47	0.00	2.55	6.96	3.15	1.64	0.93	64.70	0.69	1.71	11.13	32.87	16.70	203.50	nd

bdl below detection limit, *nd* not determined. Black schists from the upper Lesser Himalaya are in bold

lower compared to the clay fraction (Fig. 4). Brown and grey clays have more or less the same REE concentrations (200 ppm), but the grey clays show less dispersion. A dilution effect by quartz can be invoked to explain the lower REE concentrations in the silty fraction because quartz is relatively abundant in these sediments. This effect cannot however, account for the difference of concentration observed between the brown and grey clays because they share similar SiO_2 content (Fig. 3). The higher abundance of CaO in the brown clay (5–15 wt %) relative to the grey clay (CaO < 5 wt %) could partly explain the lower REE content (i.e. dilution effect by carbonate). Another possibility is that the source for the clays is different: Higher Himalayan Crystalline or Lesser Himalaya for the grey clays, Siwaliks for the brown clays. All the sediments analysed in this study show fractionated normalised REE patterns with average La_N/Yb_N ratios of 9.95, 9.74 and 9.62 for the grey clays, brown clays and sand/silt, respectively (Fig. 4). Weathering processes can explain the different REE concentrations in the sediments (e.g. Potter et al. 2005; Singh 2009). The $(Eu/Eu^*)_N$ ratio is very consistent from one sample to another, with the europium anomaly being strongly negative, varying between 0.17 and 0.23. For comparison, we report the average REE pattern of sediments from different parts of the mainstream Ganga river, after the confluence of all of its tributaries and before entering the Ganga plain (Singh 2009). It is noticeable that REE patterns of the Ganga sediments are quite similar to

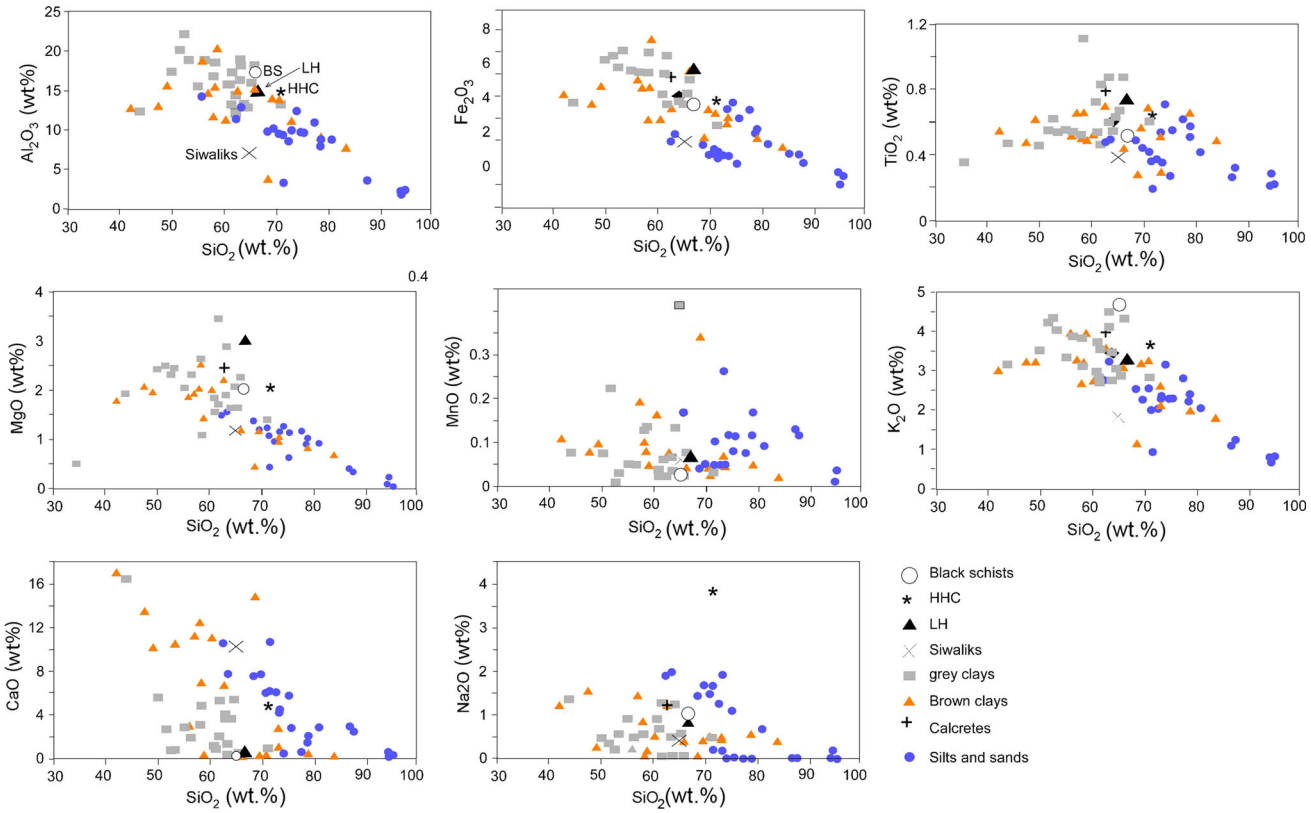

Fig. 3 Variation diagram of major elements against SiO_2 (wt %) for all the groups of sediment studied. Average composition of the source rocks are from Galy and France-Lanord (2001) including our data presented in Table 1. *THB* trans-himalayan batholith, *HHC* higher himalayan crystallines, *LH* Lesser Himalaya

the pattern of our samples, particularly for the clay fraction. However, the Ganga sediments are on average two times more enriched in HREE than the studied samples. In contrast, the average Siwaliks pattern is similar to the pattern of our three groups, and its average REE concentration is equal to the average concentration of the studied samples.

The Upper Continental Crust (UCC) (Taylor and McLennan 1985) normalised REE patterns of the studied samples are reported in Fig. 5. As already noticed by Singh (2009) for the Ganga river sediments, the significant feature of the shale normalised pattern is the depletion of Eu in the three groups of sediments, and the similarity of the REE patterns of the three groups with the Higher Himalayan Crystalline and Lesser Himalaya is highlighted. Moreover, in both REE normalised diagrams (Figs. 4, 5), the grey clays fractions representing the more evolved sediments are equally enriched compared to the Higher Himalayan Crystallines and Lesser Himalayan rocks.

Arsenic distribution

The distribution of arsenic is not uniform among sediment types. In general, arsenic concentrations are higher in the fine-grained fraction (grey clay and brown clay) than in coarser materials (fine sand and silt). This could be related to the quartz dilution effect. The average arsenic concentration in the analysed samples is 8 ppm. The average arsenic concentration in the grey clays is 11 ppm, 8 ppm in the brown clays and 4 ppm in the silt/sand fraction (Table 2). The highest arsenic concentration (27.7 ppm) is observed in the borehole 4 at a depth of 20.7 m, in a metre-thick, dark grey layer (Fig. 2). A general positive trend appears between arsenic concentration, Fe_2O_3, K_2O and Al_2O_3 contents (Fig. 6). The average total iron as Fe_2O_3 is 4.33 wt %, with higher concentrations in the clay layers (5.71 wt %) and lower concentrations in the silt/sand layers (2.76 wt %). The arsenic concentration partly increases with the total C organic content. In contrast, there is no relationship between arsenic content and calcium content. We also reported the average arsenic content of the potential sources. The black schists from the Lesser Himalaya have the highest content (14–19 ppm), the micaschists and gneisses of the Higher Himalayan Crystallines have the lowest content (0–3 ppm) while the rest of the Lesser Himalaya (0–7 ppm) and the Siwaliks (0–10 ppm) have intermediate arsenic content. In the discussion, we will show that weathering processes affecting the Lesser Himalaya

Table 3 Geochemical composition in REE elements of the Nawalparasi borehole sediments and rocks coming from Himalaya (*HHC* higher himalayan crystallines, *LH* lesser himalaya, *Siw Siwaliks*)

Samples	La (ppm)	Ce (ppm)	Pr (ppm)	Nd (ppm)	Sm (ppm)	Eu (ppm)	Gd (ppm)	Tb (ppm)	Dy (ppm)	Ho (ppm)	Er (ppm)	Tm (ppm)	Yb (ppm)	Lu (ppm)
PNS 2/10	53.20	101.00	12.10	44.40	8.61	1.59	6.94	1.10	6.27	1.26	3.61	nd	3.31	0.50
PNS 2/20	48.60	99.90	11.40	42.10	8.30	1.51	6.77	1.07	6.17	1.24	3.54	nd	3.26	0.49
PNS 2/28	32.20	65.60	7.40	28.40	5.69	1.04	4.73	0.79	4.46	0.91	2.64	nd	2.54	0.39
PNS 2/36	38.90	78.00	9.40	33.30	6.55	1.20	5.74	0.92	5.05	1.08	3.20	nd	2.81	0.43
PNS 2/49	37.60	76.50	8.80	32.00	6.35	1.00	5.21	0.85	5.06	1.00	2.92	nd	2.77	0.43
PNS 2/52	25.30	49.90	5.83	21.50	4.13	0.72	3.59	0.57	3.14	0.67	1.82	nd	1.64	0.26
PNS 2/57	42.20	81.50	9.67	35.30	6.60	1.09	5.96	0.94	5.35	1.06	3.03	nd	2.80	0.42
PNS 2/60	37.40	69.80	8.68	31.40	6.28	1.18	5.26	0.84	4.70	0.94	2.64	nd	2.40	0.36
PNS 2/62	49.20	97.00	11.40	41.20	8.19	1.52	6.62	1.06	6.10	1.21	3.57	nd	3.18	0.47
PNS 2/63	42.30	87.50	9.78	35.60	7.03	1.26	5.67	0.91	5.18	1.03	2.94	nd	2.78	0.42
PNS 2/67	45.30	86.50	10.40	38.60	7.34	1.35	5.96	0.97	5.34	1.11	3.04	nd	2.83	0.44
PNS 2/75	45.00	88.70	10.40	38.00	7.31	1.36	6.11	0.98	5.47	1.13	3.24	nd	2.92	0.44
PNS 3/10	48.30	95.70	11.30	40.70	7.67	1.39	6.16	1.02	5.85	1.23	3.49	nd	3.26	0.49
PNS 3/18	45.60	91.90	10.80	39.10	7.51	1.38	6.31	1.02	5.93	1.21	3.44	nd	3.23	0.49
PNS 3/28	52.50	107.00	12.10	44.30	8.59	1.61	7.06	1.14	6.58	1.31	3.75	nd	3.43	0.51
PNS 3/32	51.70	105.00	11.70	42.50	8.32	1.53	6.62	1.08	6.03	1.21	3.49	nd	3.20	0.49
PNS 3/37	45.20	93.30	10.60	38.60	7.48	1.45	6.23	1.00	5.89	1.18	3.35	nd	3.12	0.48
PNS 3/40	34.00	67.30	8.00	29.00	5.62	0.99	4.68	0.75	4.09	0.82	2.34	nd	2.20	0.33
PNS 3/46	31.90	62.00	7.32	27.20	5.26	0.98	4.66	0.75	4.16	0.89	2.42	nd	2.31	0.35
PNS 3/55	29.40	57.10	6.66	23.30	4.38	0.97	3.89	0.62	3.65	0.75	2.04	nd	1.95	0.30
PNS 3/60	27.10	53.40	6.28	22.70	4.43	0.86	3.69	0.60	3.41	0.70	2.06	nd	1.93	0.29
PNS 3/62	42.70	90.50	9.82	36.40	6.97	1.26	5.72	0.93	5.41	1.09	3.15	nd	3.00	0.45
PNS 3/70	44.00	89.40	10.10	36.80	6.93	1.16	5.49	0.90	5.37	1.11	3.30	nd	3.15	0.49
PNS 3/85	43.40	86.60	10.20	37.20	7.05	1.25	5.58	0.89	5.10	1.05	2.99	nd	2.78	0.43
PNS 4/17	49.20	97.90	11.50	42.00	7.99	1.43	6.54	1.07	6.04	1.26	3.62	nd	3.36	0.51
PNS 4/35	38.90	85.50	9.30	34.90	7.02	1.33	6.00	0.95	5.63	1.14	3.27	nd	3.02	0.46
PNS 4/45	36.70	74.80	8.50	30.70	6.05	1.12	5.17	0.84	4.87	0.99	2.78	nd	2.59	0.40
PNS 4/53	27.90	56.00	6.60	24.20	4.81	0.88	4.02	0.66	3.61	0.74	2.09	nd	1.89	0.29
PNS 4/60	39.20	77.90	9.08	33.20	6.28	1.13	5.19	0.84	4.76	1.00	2.92	nd	2.74	0.42
PNS 4/69	44.00	88.90	10.20	36.80	7.14	1.34	5.81	0.94	5.39	1.07	3.01	nd	2.80	0.43
PNS 4/74	43.10	86.10	9.87	36.20	7.10	1.30	5.74	0.91	5.28	1.07	2.98	nd	2.80	0.42
PNS 5/16	39.80	78.80	9.14	33.20	6.33	1.17	5.18	0.82	4.91	1.02	2.88	nd	2.68	0.42
PNS 5/19	34.40	68.80	8.13	29.50	5.62	0.97	4.72	0.75	4.45	0.93	2.76	nd	2.55	0.40
PNS 5/25	15.80	31.50	3.72	13.60	2.59	0.43	2.09	0.36	2.05	0.44	1.33	nd	1.31	0.20
PNS 5/36	38.50	76.50	8.96	33.30	6.58	1.17	5.45	0.90	5.05	1.04	2.95	nd	2.78	0.41
PNS 5/40	39.30	78.50	9.24	34.10	6.84	1.28	5.77	0.96	5.48	1.11	3.24	nd	2.96	0.45
PNS 5/42	24.20	48.30	5.70	20.70	4.18	0.76	3.69	0.59	3.47	0.72	2.07	nd	1.93	0.29
PNS 5/45	30.40	60.30	7.12	25.80	5.11	0.91	4.28	0.68	3.83	0.78	2.27	nd	2.11	0.32
TE11	41.05	79.72	8.75	34.92	7.08	1.50	6.03	0.90	4.87	0.87	2.30	0.32	1.96	0.29
TE12	43.20	85.34	9.38	37.37	7.37	1.32	6.06	0.88	4.78	0.95	2.99	0.49	3.47	0.56
TE13	34.77	68.14	7.51	30.03	6.06	1.18	5.07	0.74	3.99	0.75	2.14	0.33	2.28	0.36
TE19	36.14	71.35	7.89	31.57	6.35	1.21	5.55	0.85	4.81	0.92	2.67	0.41	2.81	0.43
TE20	41.41	76.92	8.30	32.81	6.59	1.54	5.98	0.97	5.93	1.17	3.32	0.49	3.33	0.51
TE26a	41.84	74.51	9.20	34.73	6.76	1.29	5.77	0.91	5.59	1.14	3.43	0.53	3.61	0.56
TE26b	27.50	50.55	5.15	18.91	2.96	0.35	2.08	0.29	1.67	0.32	0.96	0.15	1.07	0.18
TE27	15.96	33.49	4.11	18.44	4.46	1.46	4.44	0.68	4.03	0.77	2.13	0.31	1.96	0.30
TE28	19.04	38.10	4.55	19.91	4.45	1.40	4.29	0.65	3.85	0.72	2.01	0.30	1.91	0.30

Table 3 continued

Samples	La (ppm)	Ce (ppm)	Pr (ppm)	Nd (ppm)	Sm (ppm)	Eu (ppm)	Gd (ppm)	Tb (ppm)	Dy (ppm)	Ho (ppm)	Er (ppm)	Tm (ppm)	Yb (ppm)	Lu (ppm)
BU2	2.43	7.12	1.05	4.63	1.18	0.24	1.05	0.16	0.90	0.18	0.45	0.06	0.40	0.06
TE1	4.40	9.25	1.05	3.72	0.67	0.16	0.54	0.08	0.44	0.08	0.22	0.03	0.19	0.03
TE3	0.60	1.12	0.12	0.47	0.08	0.02	0.08	0.01	0.07	0.02	0.05	0.01	0.05	0.01
TE4	0.95	2.09	0.21	0.86	0.16	0.03	0.15	0.02	0.16	0.03	0.10	0.01	0.09	0.02
TE7	0.41	0.68	0.08	0.31	0.06	0.01	0.04	0.01	0.07	0.02	0.07	0.01	0.11	0.02
TE8	1.67	3.97	0.40	1.63	0.33	0.08	0.31	0.05	0.28	0.06	0.15	0.02	0.14	0.02
TE9a	46.46	87.95	9.45	36.44	6.75	1.30	5.60	0.86	4.89	0.93	2.58	0.38	2.33	0.34
TE9b	1.10	2.15	0.25	1.00	0.20	0.04	0.16	0.03	0.16	0.03	0.09	0.01	0.10	0.01
TE2	48.52	94.69	10.71	37.89	6.65	1.27	5.28	0.79	4.50	0.89	2.57	0.39	2.66	0.42
TE10	32.01	56.71	6.28	23.72	4.36	0.86	3.65	0.60	3.74	0.80	2.49	0.39	2.75	0.43
TE30	57.11	107.20	11.72	45.48	8.36	1.64	6.63	0.99	5.68	1.08	3.04	0.45	2.98	0.46
TE35	14.46	29.06	3.12	12.60	3.12	0.60	3.70	0.56	3.16	0.59	1.67	0.25	1.60	0.24
TE21	24.24	47.67	5.22	20.56	4.02	0.86	3.47	0.53	3.21	0.63	1.83	0.28	1.91	0.30
TE23	25.92	51.35	5.51	21.43	4.26	0.81	3.69	0.58	3.44	0.67	1.92	0.30	1.94	0.29
TE24	39.10	73.08	8.10	30.87	5.44	1.11	4.14	0.61	3.44	0.65	1.78	0.25	1.61	0.23
TE18	53.92	100.20	10.32	38.40	6.66	1.37	5.17	0.76	4.31	0.83	2.34	0.37	2.52	0.39
TE29	11.29	16.35	1.52	5.35	0.78	0.19	0.50	0.07	0.39	0.07	0.21	0.03	0.24	0.04
TE31	15.69	33.39	4.20	19.09	4.43	1.76	4.59	0.71	4.25	0.81	2.22	0.32	2.05	0.32
TE32	4.45	10.13	1.04	4.26	0.85	0.15	0.76	0.12	0.72	0.15	0.41	0.06	0.43	0.07
TE33	0.41	0.86	0.10	0.41	0.08	0.01	0.06	0.01	0.06	0.01	0.03	0.01	0.03	0.01
TE34	33.44	64.97	7.09	27.71	5.18	0.93	4.26	0.66	3.93	0.77	2.31	0.35	2.39	0.39
TE36	9.19	18.29	2.25	9.46	2.31	0.50	2.17	0.29	1.58	0.29	0.78	0.11	0.70	0.11
TE37	43.82	85.43	10.33	40.91	8.47	1.69	7.64	1.18	6.67	1.31	3.67	0.53	3.59	0.56
TE38	60.45	184.80	23.03	93.86	19.56	3.32	14.93	1.85	8.55	1.37	3.30	0.43	2.65	0.41
TE39	50.15	98.45	10.86	40.44	7.45	1.32	6.15	1.00	6.02	1.21	3.50	0.52	3.60	0.56
TE40	41.27	98.53	10.65	43.97	10.03	2.28	9.91	1.54	8.73	1.64	4.37	0.61	4.08	0.64
TE41	22.84	43.63	5.10	18.93	3.83	0.75	3.42	0.53	3.09	0.60	1.72	0.25	1.69	0.26
TE42	28.90	57.34	6.55	24.20	4.75	0.85	3.95	0.61	3.49	0.67	1.91	0.28	1.95	0.31
TE44	30.75	60.43	6.89	25.67	5.06	1.00	4.42	0.71	4.04	0.78	2.22	0.33	2.23	0.35
TE45	34.41	67.97	7.69	28.50	5.52	1.05	4.62	0.73	4.28	0.83	2.40	0.36	2.44	0.38
TE47	34.41	66.64	7.58	27.45	4.96	0.93	3.83	0.57	3.15	0.58	1.64	0.24	1.67	0.27
TE48	1.60	3.16	0.36	1.29	0.24	0.04	0.20	0.03	0.18	0.04	0.10	0.01	0.09	0.01
TE50	29.41	62.44	6.89	26.84	5.49	1.28	4.66	0.71	4.22	0.80	2.26	0.33	2.28	0.34

nd not determined. Black schists from the upper Lesser Himalaya are in bold

black schists most likely explain the arsenic enrichment observed in the grey clays.

Shell geochemistry

Fragments of shell of freshwater mollusks were collected from the sledge samples at eight different depths below ground level and belong to *Gastropod* sp, *Bellamya* sp., and *bivalvia* sp. Carbon ($\delta^{13}C$) and oxygen ($\delta^{18}O$) isotope values of these shells range from −7 to +2 ‰, and −9 to −3 ‰, respectively, in PDB scaling (Table 2). One living freshwater mollusk of *Lymnaea* sp. was also sampled on 8 May 2007 from 2 m wide and 0.15 m deep running river water of the Turia Khola at Amahawa (27°30′55″N, 83°36′11″E; 106 m a.m.s.l.). Temperature and pH value of the water were, respectively, 32.9 °C and 8.33. The $\delta^{13}C$ and $\delta^{18}O$ values of the shell are, respectively, −9.3 and −3.8 ‰ (Table 4).

Discussion

Stratigraphy and dating

The stratigraphy and depositional history of Quaternary sediments in the Himalayan foreland basin have been

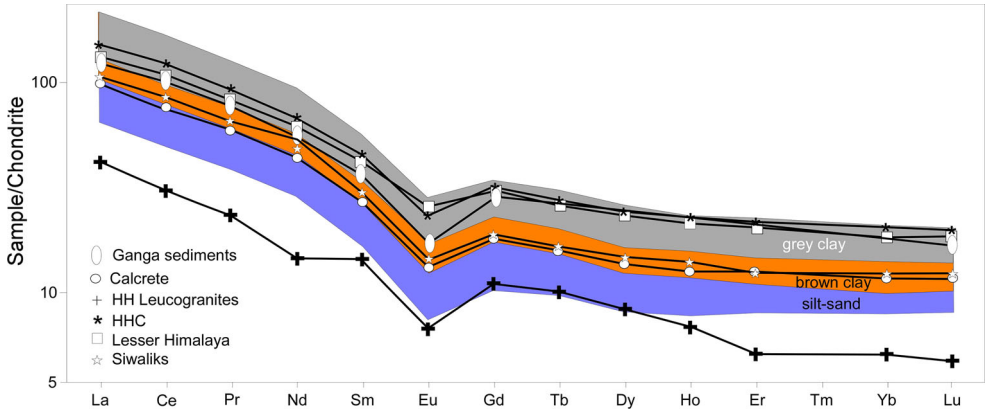

Fig. 4 Chondrite (McDonough and Sun 1995) normalised REE patterns of the Nawalparasi sediments. Average composition of potential source rocks is also reported including our data presented in Table 3. *HHL* higher himalayan leucogranites (Guillot and Le Fort 1995; Ayres and Harris 1997); *HHC* higher himalayan crystallines (Harris and Inger 1992); *LH* Lesser Himalaya (Rashid 2002). Siwaliks (C. France-Lanord, unpublished data). The average compositions of modern Ganga sediments (Singh 2009) are also reported

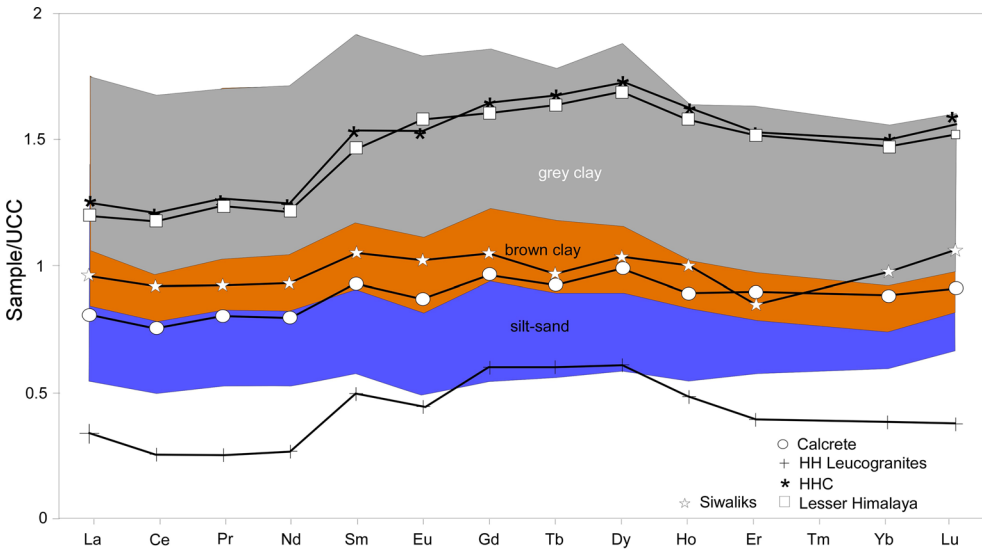

Fig. 5 Upper crust (Taylor and McLennan 1985) normalised REE patterns of the Nawalparasi sediments with average composition of potential source rocks (same reference as Fig. 4)

previously investigated (Sharma et al. 2004; Gurung et al. 2005; Shah 2008; Singh 2009). In general, these investigations show that sediment deposition has been affected by climate change during the Pleistocene–Holocene period (Sinha and Friend 1994; Sharma et al. 2004). Additionally, studies dealing with arsenic contamination of groundwater in the Bengal fan (e.g. McArthur et al. 2001; Ishiga et al. 2000; Charlet and Polya 2006) have demonstrated that high arsenic concentrations are restricted to Holocene sediments rich in organic matter. Here we correlate the stratigraphy of the Terai sediments with the Bangladesh sediments and discuss how past climatic conditions can change the aquifer lithology and arsenic concentrations.

The wood fragment from 7 m depth in borehole 5 gives a ^{14}C age between 3354 and 2928 year BC (Table 4). This age is confirmed by Gurung et al. (2005), who also obtained a little earlier ^{14}C age of 3340 ± 70 years BP from a 4 m depth in ND-2 borehole, 2 km ENE from Unwach village (Fig. 1). We also use Gurung et al.'s (2005) findings of a 12,680 ^{14}C BP aged black mud deposit to assign a date to a similar continuous black mud unit found in the Parasi transect just above 15 m (i.e., boreholes 1 and 3 "lake deposits" in Fig. 2). The depositional environment for all black clay beds may be similar and these beds can be regarded as markers. A black clay layer is also recognized in the Ganga plain at 13,030 ± 114 ^{14}C year BP in the Sanaki Lake, Central Ganga Plain (Sharma et al. 2004) but also in Bangladesh at around 12,000 year BP (Acharyya et al. 2000). Overall, we interpret the shared extent and ages of the black clays as the transition from the end of Late Glacial Pleistocene period and the beginning of the warmer Holocene period starting ~12,000 year BP (Zhao et al. 1995).

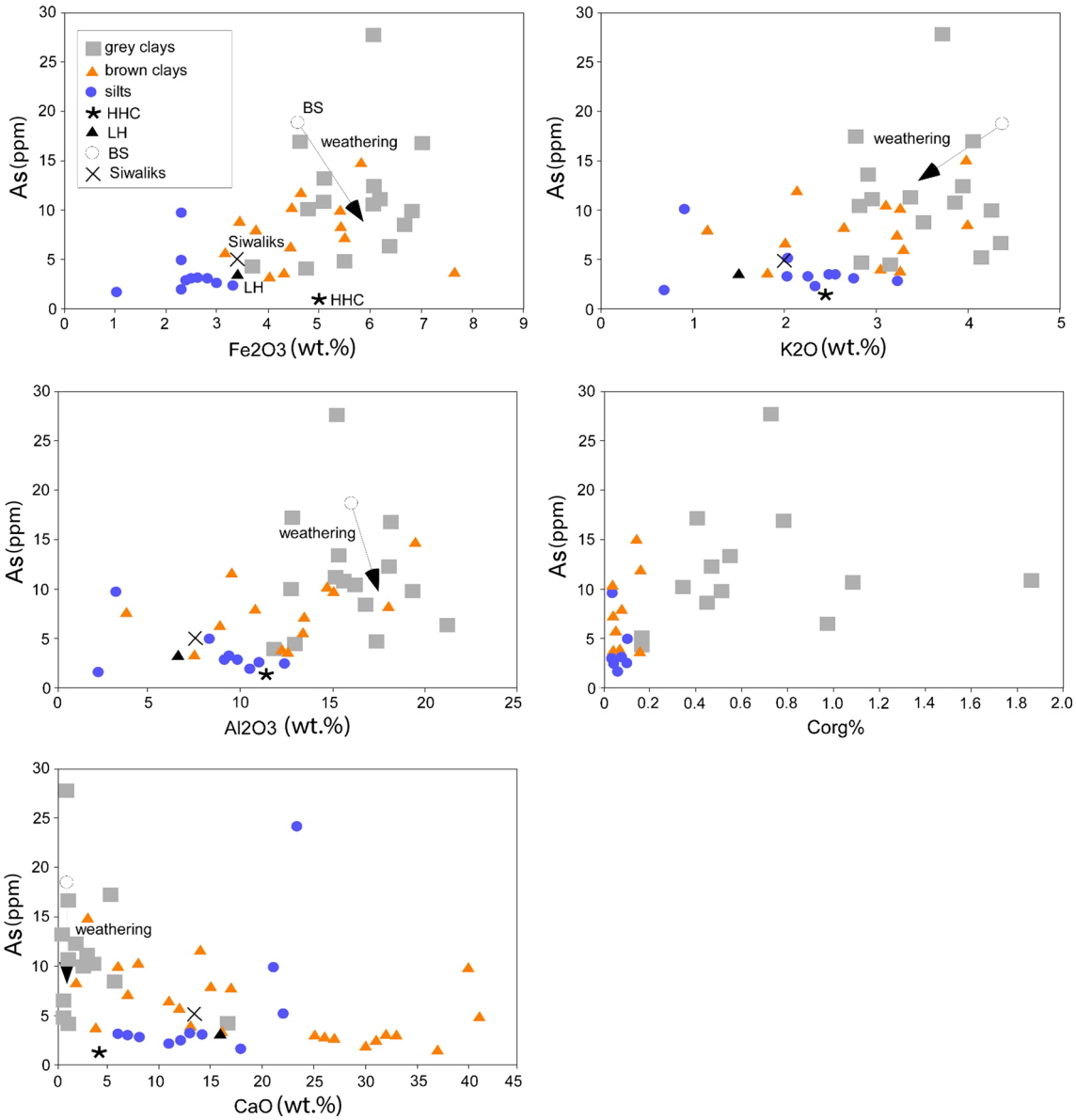

Fig. 6 Variation diagram against the arsenic content. Average composition of the source rocks is from Galy and France-Lanord (2001) including our data presented in Tables 1 and 2. *HHC* higher himalayan crystallines, *LH* lesser himalaya, *BS* black schists

Provenance

Previous studies of the Indo-Gangetic plain, mostly based on bedload and suspended-load composition (Galy and France-Lanord 2001), have suggested that Higher Himalayan Crystallines form the major source of the Ganga plain sediments with the Lesser Himalaya contributing to only 10–20 % of the sediment load. In contrast, Tripathi et al. (2007) proposed that the REE homogeneity of the Ganga Plain sediments shows a high degree of sediment homogenization through several episodes of sedimentary reworking and proposed that they most likely represent the reworking of Siwalik sediments. Moreover, Huyghe et al. (2005) show that the major source for the Tertiary Siwalik sediments is the Higher Himalayan Crystallines, and thus it remains difficult to discriminate if the Ganga plain sediments derive directly from the Higher Himalayan Crystallines or if they are reworked from the Siwaliks sediments. To depict the chemical changes recorded by the sediments from the source region to the deposition site, it is first necessary to evaluate element mobility. This allows us to discriminate between the changes controlled by physical processes, such as sorting, and changes due to chemical weathering. For that we used the method of Fralick and Kronberg (1997) reactualised by Lupker et al. (2012) based on binary diagrams using elements suspected to be

Table 4 $\delta^{13}C$ and $\delta^{18}O$ data of the mollusk fossil collected from drill samples of Nawalparasi, Nepal

Samples	Location	Coordinate (latitude/longitude)	Depth below ground level (m)	$\delta^{18}O$ (PDB) ‰	$\delta^{13}C$ (PDB) ‰	Genus
Dril 1/52–53′	Suspurwa	27 30 54.3N/83 40 25.8E	16.0	−2.7	+1.0	*Gastropod* sp.
Dril 1/55–60′	Suspurwa	27 30 54.3N/83 40 25.8E	17.5	−9.0	−6.6	*Bellamya* sp.
PNS 2/55′	Unwach	27 31 00.5N/83 40 37.4E	16.5	−7.8	−3.5	*Gastropod* sp.
PNS 2/65B′	Unwach	27 31 00.5N/83 40 37.4E	19.5	−5.9	+0.8	*Bellamya* sp.
PNS 2/67′	Unwach	27 31 00.5N/83 40 37.4E	20.1	−2.8	+1.5	*Gastropod* sp.
Dril 4/72′	Jeetpur	27 30 58.3N/83 39 48.1E	22	−3.4	+1.1	*Gastropod* sp.
Dril 4/74′	Jeetpur	27 30 58.3N/83 39 48.1E	22.5	−3.5	−0.1	*Bivalvia* sp.
PNS 5/14′	Santapur	27 30 55.0N/83 40 3.8E	4.6	−8.0	−4.9	*Gastropod* sp.

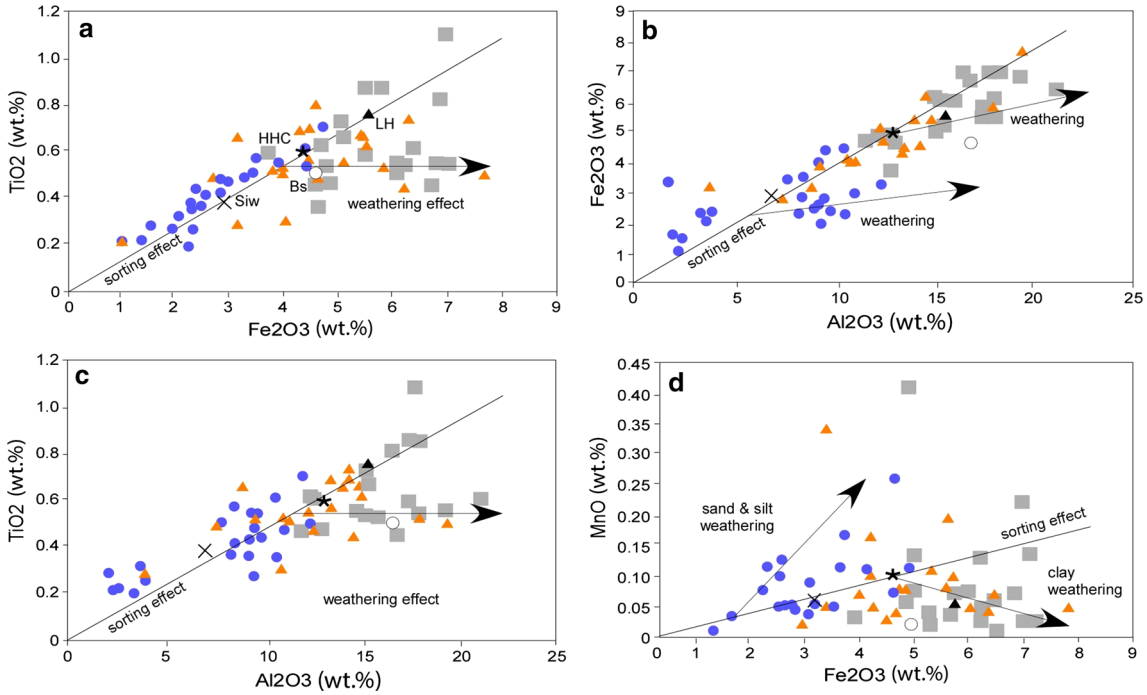

Fig. 7 Plots of sediments in the bivariant diagram between two immobile elements. Average compositions of the source rocks are from Galy and France-Lanord (2001) including our data presented in Table 1. The *trend line* including the HHC and the *origin* shows the effect of hydraulic sorting whereby the above group of elements concentrate in finer fraction and are depleted in the coarser fraction. The *points* plotting far for this line show the weathering effect. The *symbols* and *abbreviations* are the same as Fig. 6

immobile. The binary graphs plot elements against SiO_2 (Fig. 3), gives a first indication about the sediment's hydraulic behaviour and element mobility. Except for Na_2O, CaO and MnO, the other elements define a negative linear array extending towards 100 % SiO_2. This indicates that these elements are more chemically immobile and only record sorting effects as they concentrate in the finer (clays) fractions. In contrast, Na_2O, CaO and MnO show depletion in the finer fractions, suggesting that their concentrations should be more sensitive to and predictive of chemical weathering.

In the binary diagrams (Fig. 7), ~70 % of the samples define a linear array along a line extending towards the origin. This demonstrates that TiO_2–Fe_2O_3–Al_2O_3 were mostly immobile and hydraulically fractionated in a similar way. Along these lines, the effect of hydraulic sorting is highlighted with the highest concentration of elements in the finer fraction (clays) and depleted in coarser fraction (silt and sand). Considering the linear arrays defined in the Figs. 3 and 7 and the similar REE patterns defined by the four groups of elements (i.e. grey clays, brown clays, calcretes and silts), we suspect that the studied sediments are

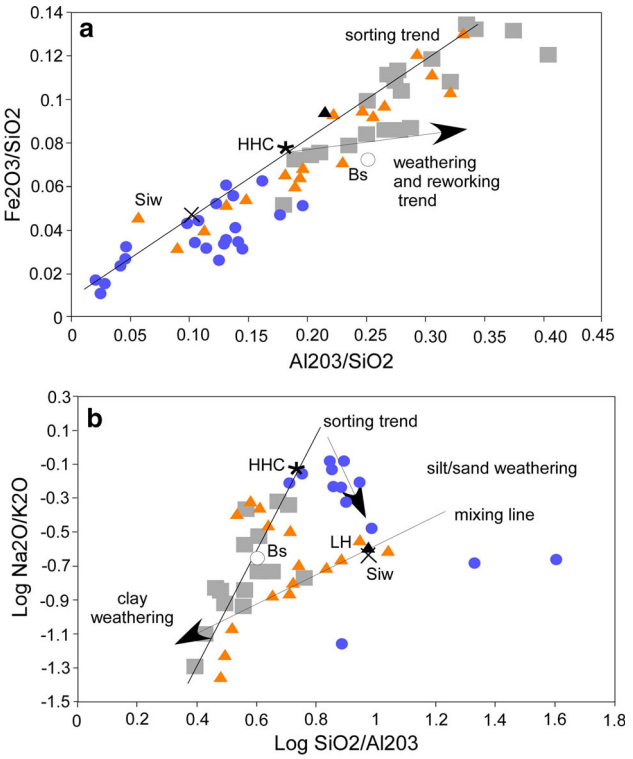

Fig. 8 Plot of sediments in Fe_2O_3/SiO_2 vs. Al_2O_3/SiO_2 and Log Na_2O/K_2O vs. log SiO_2/Al_2O_3 diagrams showing the pathway of chemical evolution of feldspar from the source to the plain. Average compositions of the source rocks are from Galy and France-Lanord (2001) including our data presented in Table 1. The *symbols* and *abbreviations* are the same as Fig. 6

mainly derived from the same dominant source or sources having similar chemical composition. Moreover, in a binary diagram of two immobile elements (Fig. 7), it is expected that the plots of both finer and coarser sediments will move away in opposite direction and the tie lines joining them will pass through their common source (Fralick and Kronberg 1997). Among the potential sources, only the Higher Himalayan Crystallines and Lesser Himalaya meet this criteria (Fig. 7). However, some grey clay and a few brown clays are enriched in Fe_2O_3 and Al_2O_3 and define a second line passing through the black schists. This suggests that these samples specifically derived from the weathered Lesser Himalaya black schists.

Similarly, in a Fe_2O_3/SiO_2–Al_2O_3/SiO_2 diagram (Fig. 8a), all sediments cluster around the average composition of the Higher Himalayan Crystallines and Lesser Himalayan rocks, suggesting, here again, a predominant contribution from these two sources. The lability of plagioclase relative to K-feldspar and of K-feldspar relative to quartz results in substantial modification to the quartz: plagioclase: K-feldspar proportions by weathering processes; thus, the plot Na_2O/K_2O versus SiO_2/Al_2O_3 can be used to assess the behaviour of feldspars (Nesbitt et al. 1997). In Fig. 8b, we also observe that about 50 % of the samples plot along a linear array including the average Higher Himalayan Crystallines and Lesser Himalaya black schist composition. This trend reflects feldspar sorting in suspended sediment during fluvial transport (Nesbitt et al. 1997). We observe again that Siwaliks and Lesser Himalaya are well separated from the trend related to feldspar sorting, indicating that the Higher Himalayan Crystalline rocks and black schists from the Lesser Himalaya are the predominant contributors to the Parasi sediments. The other 50 % of the samples, including most of the silt/sand samples and most of the brown clays, plot outside the linear trend suggesting weathering, reworking, and possible input by the Siwaliks.

REE elements can also be used to assess the source rock composition (Taylor and McLennan 1985). All the sediments in this study show fractionated normalised REE pattern with average La_N/Yb_N ratio of 9.95, 9.74 and 9.62 for grey clays, brown clays and sand/silt, respectively. Those values are similar to modern sediments from the Narayani (La_N/Yb_N ratio of 9.1) and the Ganga (9.9) according to Garçon et al. (2013). Deeper Eu anomalies compared to UCC suggest more silicic source than average continental crust (Fig. 5). Lesser Himalayan and Higher Himalayan Crystalline rocks share similar pattern with the Parasi clay sediments confirming that they are the main sources (Fig. 5). According to the compilation of available REE data done by Garçon et al. (2013), the La_N/Yb_N ratio of the Parasi sediments are closer to the La_N/Yb_N ratio of the Lesser Himalaya derived-sediments (11.3) than to that of the Higher Himalayan Crystallines derived-sediments (4.2), but very close to Siwaliks La_N/Yb_N ratio (9.09). Considering that the REE concentrations in the sources and in the sediments are similar (150 ± 50 ppm), the La_N/Yb_N ratio in the sediments and the dominant sources (Higher Himalayan Crystalline and Lesser Himalaya) can be used as a proxy to estimate their respective contribution in the Parasi sediments. Considering that the Upper Himalaya and the Siwaliks contribute to a maximum of 40 % of the sediments in the flood plain (Garzanti et al. 2007),we estimate that the uppermost part of the Lesser Himalaya contributed at 45 % and the lower part of the Higher Himalayan Crystallines only at 15 %.

This estimate is in contradiction with previous provenance studies on the Ganga plain sediments, (Galy and France-Lanord 2001; Singh 2009) suggesting that the Higher Himalayan Crystallines is the major source and that the Lesser Himalaya contribute to only 20 % of the sediment load. Based on petrological and mineralogical studies on modern sediments in the Marsyandi river catchment in central Nepal (Fig. 1), Garzanti et al. (2007) proposed that most of the Ganga sediments derived from the lower part of the Higher Himalayan Crystallines, within the Main

Central Thrust zone where annual rainfall is maximum at 3000 m and reaches 5 m/year. Thus, erosion rate is maximum and quite high in this part of the Higher Himalayan Crystallines, estimated at 5.1 ± 1.2 mm/year. However, Amidon et al. (2005) show ~3 times higher modern erosion rates south of the Main Central Thrust in the northernmost Lesser Himalaya where the black schists outcrop. Present-day erosion rates also decrease in the upper part of the Higher Himalayan Crystallines to the north despite the extreme topography with 7000–8000 m peaks, because precipitation is too scarce to feed significant ice flux and glacial activity (Harper and Humphery 2003). Southwards, in the Lesser Himalaya and Siwaliks, erosion rates are markedly lower (3 times lower) because rainfall decreases and relief is lower (Garzanti et al. 2007).We conclude then, that at the front of the Himalayan belt, Pleistocene/Holocene sediments in the Terai plain in Central Nepal resemble modern sediments of the Gangetic alluvial plain and the main Himalayan river catchments from the upstream Narayani including the Kali Gandaki and Marsyandi reaches. Sediments shed from these source areas are geochemically dominated by the uppermost part of the Lesser Himalaya and the lowermost part of the Higher Himalayan Crystalline because of focused erosion related to rapid uplift and high rainfall in the Main Central Thrust zone (Lavé and Avouac 2001).

Weathering effects

As already discussed, the chemistry of sediments is controlled by provenance but also by weathering and fluvial processes (McLennan et al. 1993; Singh 2009).

The A-CN-K triangular plot of Nesbitt et al. (1997) gives the weathering trend for the sediments (Fig. 9). All the sediments plot along the same weathering line, confirming their similar provenance. The silty fraction plots near the K-feldspar line and on the lower side of the field of the Higher Himalayan Crystallines source rocks. This suggests that these sediments are chemically unweatheared, and the shift towards the CN end-member reflects sorting effect with reduction of aluminosilicates phases remaining in the suspended load. They define a linear trend similar to the upper reaches sediments of the modern Ganga system. On the other hand, grey clays plot at the higher side of the source field indicating strong weathering may be in the suspended load or after entering into the plains by breakdown of the feldspar fraction, and hence loss of CaO and Na_2O. Compared to the modern Ganga interfluve sediments that are the more mature sediments, the grey clays plot above, again suggesting more drastic weathering. In between, the brown clays plot in intermediate position.

To better separate the effects of sorting versus weathering, some of the other diagrams are useful. Using Fig. 7a,

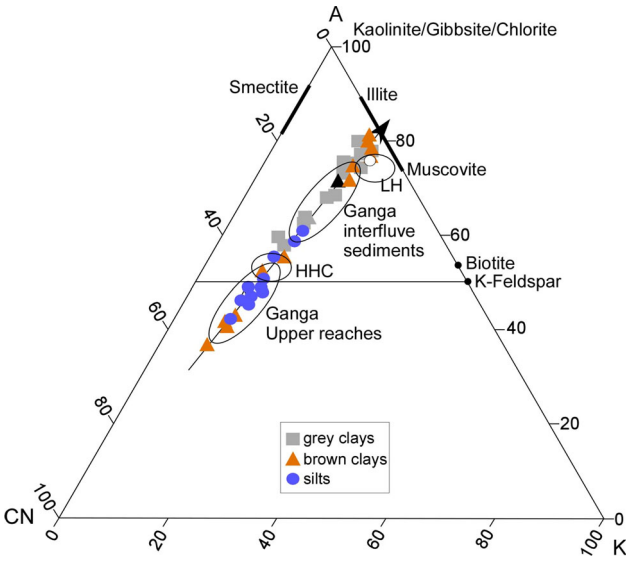

Fig. 9 A-CN-K plots (Nesbitt et al. 1997) for sediment samples. Average compositions of the source rocks are from Galy and France-Lanord (2001) including our data presented in Table 1. Ganga sediments are from Singh (2009). Notice that the Nawalparasi clays are much more weathered than the modern Ganga interfluve sediments suggesting more drastic weathering conditions than today

b, and c, 30 % of the samples do no plot on the line showing this more intense weathering effect. Fe_2O_3 and Al_2O_3 are enriched mostly in the grey clay fractions, while decreases in SiO_2 content, Na_2O and CaO (Fig. 3) is symptomatic of alteration of gneissic rocks under tropical conditions (Tardy and Nahon 1985). In contrast, some coarse sediments are only enriched in Al_2O_3; as they intersect the tie line in its lower part (Fig. 8b), Al_2O_3 enrichments in the silts suggest that they weathered under different conditions. This hypothesis is confirmed by Fig. 7d. In this diagram, sand and silt are enriched in MnO relative to Fe_2O_3 while clays are depleted in MnO relative to Fe_2O_3. This reflects contrasting redox conditions during weathering, with more reduced conditions present during grey clay weathering. As Fe concentrations are higher than Mn, the majority of the soil cations exchange complex in reduced conditions is occupied by Fe^{2+}, thus leaving Mn^{2+} ions in solution. In contrast, in the silt/sand fraction, oxic conditions precipitated Mn according to the reaction (Reddy and DeLaune 2008):

$$2Mn^{2+} + O_2 + 2H_2O = 2\,MnO_2 + 4\,H^+$$

As already discussed, the Na_2O/K_2O versus SiO_2/Al_2O_3 plot (Fig. 8b) reflects feldspar behaviour during sorting but also weathering processes. 50 % of the samples, including most of the silt/sand samples and a large portion of the brown clays, plot outside of the linear trend suggesting reworking processes. The upper linear trend reflects sorting processes with higher concentration of Na_2O in the coarser sediments, whereby aluminosilicates (mostly micas, chorite

and illite) are preferably taken in the suspended load, resulting in increased K_2O and Al_2O_3 along the trend line (Galy and France-Lanord 2001).

In the diagram Al_2O_3/SiO_2 vs. K_2O/SiO_2 (Fig. 10), we report the evolution of the studied samples compared to modern river sediments covering the whole Ganga basin from the Himalayan front in Central Nepal to Bangladesh (data from Lupker et al. 2012). Most of our samples, except the grey clays, plot along the Himalayan front linear array reflecting sorting effect without any evidence of chemical weathering. The grey clays and some brown clays are shifted downward towards the Ganga plain linear array, suggesting a loss in K_2O and a slight enrichment in Al_2O_3. Lupker et al. (2012) interpreted this K_2O loss in modern Ganga sediments as reflecting chemical weathering in the flood plain because of a longer residence time under wet tropical conditions. Moreover, grey clays are enriched in organic carbon (Fig. 6). This can reflect successive weathering from source rocks to plain deposits in the presence of organic matter (Meharg et al. 2006) or, alternatively, the initial content of organic carbon in the source zone because the black schists contain up to 30 % of carbon (Paudel 2012). In continental mudstones, maroon to purple colours appear to be mostly early diagenetic in origin and form by alternative wetting and drying on food plains in semi-arid to arid climates, where little organic matter is buried. In contrast, wet local conditions and abundant vegetation favour greyer facies (Potter et al. 2005). Finally, the lower MnO concentrations in the grey clays fraction suggest weathering under reduced conditions. Thus, we conclude that the grey clays, enriched in organic carbon, were possibly developed by wet weathering processes under reduced conditions.

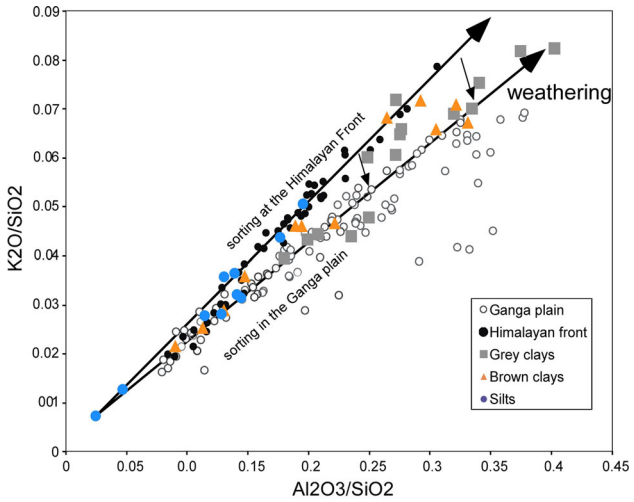

Fig. 10 Evolution of the K_2O/SiO_2 ratio as a function of Al_2O_3/K_2O, showing a depletion in K_2O and a slight enrichment in Al_2O_3 from the Himalayan front rivers downstream to the Ganga plain in Bangladesh (data from Lupker et al. 2012). We reported our samples in this diagram showing the weathering effect in the foot plain. Average compositions of the source rocks are from Galy and France-Lanord (2001) including our data presented in Table 1

Relationship between sedimentation, arsenic content and climate evolution

The climatic condition of the sedimentary environment during the deposition of the sediments in the inter-fan area of Nepal's Narayani and Tinau Rivers has oscillated between humid and arid regimes as depicted by the stable isotopic composition of the mollusk fossils (Fig. 11). The stable isotopic compositions of freshwater mollusk shells have been used to characterize the climatic conditions associated to sedimentary environments in the Indo-Gangetic plain (Gurung et al. 2005; Gajurel et al. 2006; Sharma et al. 2004). The average $\delta^{13}C$ and $\delta^{18}O$ values of modern freshwater mollusk shells in the Indo-Gangetic plain are reported as −9.5 and −7.4 ‰, respectively. The $\delta^{13}C$ values in the Parasi drilling biogenic sediments are outside of $\delta^{13}C$ from the surface shell, and $\delta^{18}O$ values are otherwise highly deviated from the reported averages (Fig. 11). The enriched C and O isotopic compositions of the biogenic carbonate possibly indicate a dry climatic regime, while the depleted values potentially suggest more humid climatic condition. This is relative to $\delta^{13}C > -7$ ‰, and $\delta^{18}O > -4$ ‰, which are modern values (Fig. 11).

Three arid periods are clearly recognized at 23.5, 20 and 11 m. These periods coincide with relatively higher arsenic content, up to 30 ppmat 20 m depth (Fig. 11). Using our ^{14}C age data, with the data of Gurung et al. (2005), we approximately date these periods at <22 kyr BP for the two oldest periods (23.5 and 20 m depth) and at 12 kyr BP, at the Pleistocene–Holocene transition for the youngest period at 11 m. The transition from arid to more humid period at 17–18 m agrees with a ~22 kyr isotopic arid-humid transition recorded in marine cores (Hayashi et al. 2008; Gibling et al. 2005; Reichart et al. 1998; Tzedakis et al. 1997) and by a decrease in the extent of glaciations in the Nepal Himalaya due to reduced precipitation (Finkel et al. 2003; Tsukamoto et al. 2002). Between 18 and 16 m depths, the $\delta^{13}C$ and $\delta^{18}O$ in the fossil shells strongly decrease, suggesting a more humid period preceding the Pleistocene's Late Glacial Maximum (Zhao et al. 1995).

Above the Pleistocene series, the development of the 2 m thick black clay layers is observed from the Terai to the Bengal fan and well dated between 13 and 10 kyr BP (Sharma et al. 2004; Gurung et al. 2005). It marks the beginning of the Holocene period and its warmer and humid climate. Nevertheless, the upper 13 m thick sedimentary deposit was also accumulated during several humid and arid climatic oscillations (Zhao et al. 1995; Sharma et al. 2004). Moreover, the boundaries between humid and

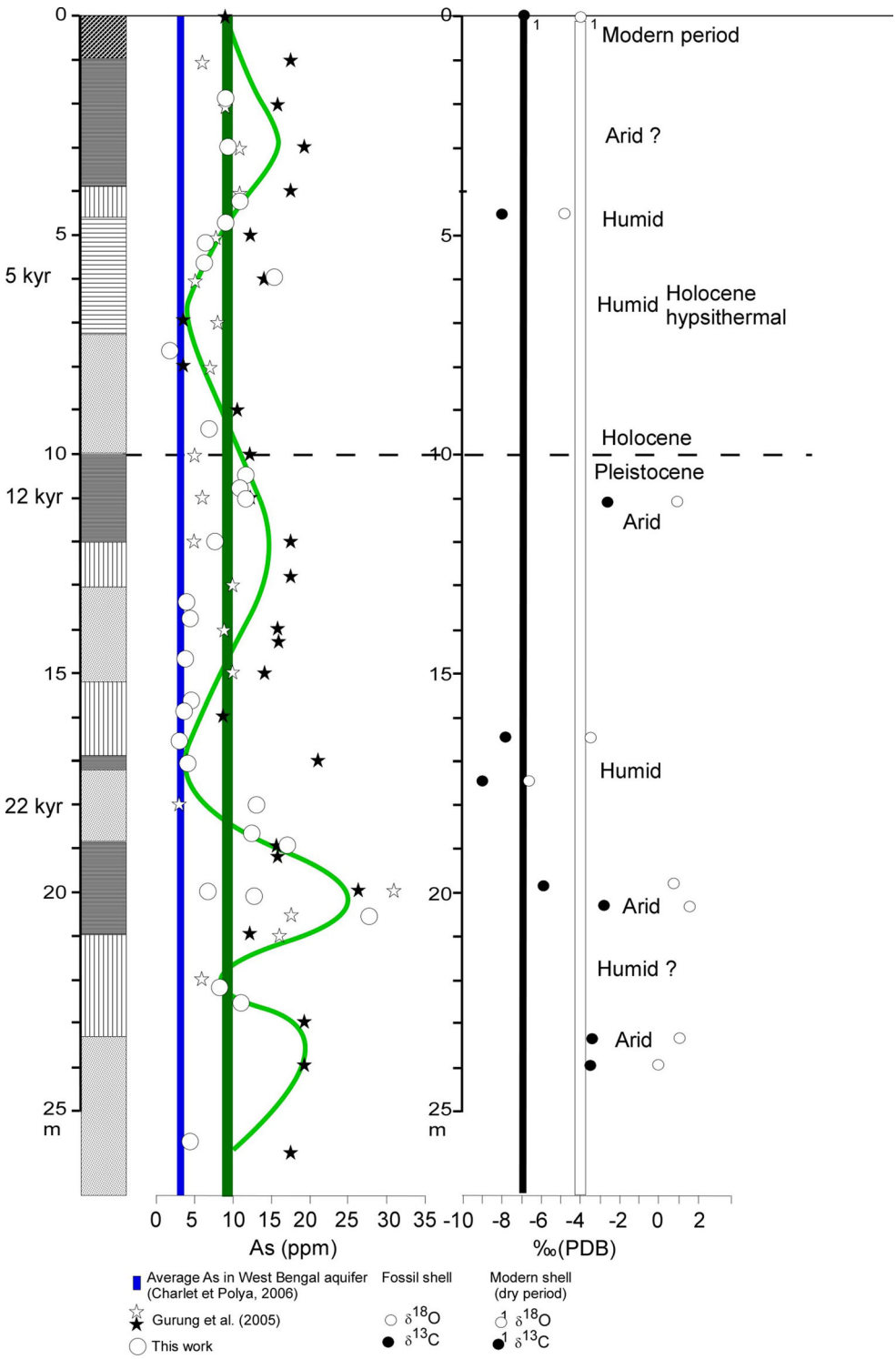

Fig. 11 Synthetic log of the Nawalparasi area showing the relationship between the lithology along the five studied boreholes and the boreholes studied of Gurung et al. (2005), the arsenic concentration the C and O isotopes and the inferred climate variation (see text for "Discussion")

arid climatic oscillations in the area are generally marked by calcrete bearing paleosols (Figs. 2, 11). At about 6 kyr BP, the monsoon intensification was five times higher that of today (about 200 mm/year) in India (Bryson and Swain 1981) corresponding to the worldwide optimum climatic (Kaufman et al. 2004). During this period, in the Nawalparasi area, an important amount of point bar and overbank sediments with lacustrine facies, as those occurring between 8 and 13 m depth, were deposited (Fig. 2) and the sediment-arsenic content remains low to very low (Fig. 11). Towards the upper part of the section, a significant calcrete bearing paleosol with dominant overbank deposits was developed at around 4 m depth that can coincide with the period of reduced monsoon precipitation in

Midlands of Nepal between 2.3 and 1.5 kyr BP (Denniston et al. 2000) and corresponds to a slight increase of the arsenic content at 6 m depth (Gurung et al. 2005).

The relationship between past sedimentary environments and the climatic regimes for the concentration of arsenic in the Parasi sediments is an important aspect that needs to be addressed to understand how arsenic accumulates in the Indo-Gangetic plain. In most of the sedimentary rocks (e.g. Smedley and Kinniburgh 2002), arsenic is concentrated in finer clay fractions, possibly reflecting accumulation in secondary iron or aluminium oxide phases. Indeed, we observe a good relationship between Al_2O_3, Fe_2O_3 and arsenic content in the studied sediments (Fig. 6). Moreover, we also observe a rather good correlation between K_2O and arsenic content, suggesting that biotite or almost-weathered biotite contributed to the fixation of this element (Nath et al. 2009). Similarly, a rough relationship exists between the organic content and the arsenic content (Fig. 6). In contrast, no relationship is observed between MnO, CaO, and P_2O_3, suggesting that ferromanganese nodules, carbonates, or apatite do not contribute to the arsenic enrichments in clay minerals, as observed in the Bengal fan sediments (Smedley and Kinniburgh 2002; Plant et al. 2003; van Geen et al. 2008).

As previously discussed, there is likely a correlation between the late Quaternary climate conditions and the concentration of arsenic in the sediments; arsenic is observed to preferentially concentrate in sediments deposited during more arid periods. The lower arsenic concentrations in sediments plain during humid periods can be explained by the process of arsenic eluviations in sandy and silty sediments due to intense summer monsoon rain during interglacial periods (Gourlan et al. 2010). Three factors seem to dominantly explain the enrichment of arsenic during the arid periods in the grey clays. Arsenic concentrates in clay sediments, associated with specific elements (FeO, Al_2O_3, K_2O and C) and linked to the degree of alteration (Fig. 6). In arid periods, when the rainfall was reduced, there was minor terrigenous clastic input from the Higher Himalayan Crystallines relative to the black schists from the Lesser Himalaya but also from watershed soil erosion, which favoured the development of swamp lands in the Ganga plain (Sharma et al. 2004). This environment favoured the development of aquatic plants and bacteria growing within the moist land areas, enhancing the strong weathering of initially suspended load particles (micas, clays), which were preferentially deposited inquiet hydraulic environments. In this environment, clays mostly deriving from C-rich black schists are chemically weathered losing Na_2O and K_2O relative to the source and relatively enriched in immobile elements such as Al_2O_3 and Fe_2O_3. During this chemical weathering process, arsenic remains relatively immobile until reduced conditions persist. Nevertheless, except in one sample, we do not observe an over-enrichment in arsenic compared to the source.

Conclusion

The average arsenic concentration in the Terai sediments is within the range of normal sediments (8 ppm) but the distribution is not homogeneous throughout the local aquifer. Abundances are greater in finer sediments, particularly in the black to grey clays (maximum 27 ppm) than in coarser silts and fine sands (3 ppm). A positive correlation exists between arsenic concentrations and clay content. In contrast, there is no correlation between arsenic and calcium content. The sediments represent homogeneous mixtures of parent rocks of felsic origin. Correlation diagrams of major elements and REE patterns suggest that the dominant source of the Late Pleistocene to Early Holocene sediments was the uppermost part of the Lesser Himalaya and the Higher Himalayan Crystalline with a possible input from the Siwaliks. In this context, the dominant source of arsenic in the present-day aquifer is the black schists from the Lesser Himalaya. The results of O and C isotopic analyses indicate a possible linkage between late Quaternary climate conditions and concentration of arsenic in the sediments. During the last $\sim$25 kyr BP, arsenic seems to be preferentially concentrated in sediments deposited during arid periods. Lower arsenic concentrations during more humid periods can be explained by a process of arsenic eluviations in sandy and silty sediments. In contrast, during dry periods, the seasonal precipitation was smaller leading to local wetter soils. This environment favoured the development of aquatic plants and bacteria growing within the moist land areas, enhancing the strong weathering of initially suspended load particles (micas, clays), which were preferentially deposited in quite hydraulic and reduced environments.

Acknowledgments The research project was supported by NSF, the CNRS INSU EC2CO and Labex OSUG20@20 programs. We acknowledge James W. LaMoreaux and the two anonymous reviewers for fruitful comments.

References

Acharyya SK, Lahiri S, Raymahashay BC, Bhowmik A (2000) Arsenic toxicity of groundwater in parts of the Bengal basin in India and Bangladesh: the role of Quaternary stratigraphy and Holocene sea-level fluctuation. Environ Geol 39:1127–1137

Amidon WH, Burbank DW et al (2005) U-Pb Zircon ages as a sediment mixing tracer in the Nepal Himalaya. Earth Planet Sci Lett 235:244–260

Ayres M, Harris N (1997) REE and Nd-Isotope fractionation during crustal anatexis: constraints from Himalayan leucogranites. Chem Geol 139:249–269

Bryson RA, Swain AM (1981) Holocene variations of monsoon rainfall in Rajasthan. Quat Res 16:125–145
Charlet L, Polya D (2006) Arsenic in shallow reducing groundwaters in southern Asia: an environmental health disaster. Elements 2:91–96
Chauvel C, Bureau S, Poggi C (2011) Comprehensive chemical and isotopic analyses of basalt and sediment standards. Geost Geoanal Res 35:125–143
Colchen M, Le Fort P, Pêcher A (1986) Recherches géologiques dans l'Himalaya du Népal. Annapurna, Manaslu, Ganesh. Paris: Ed. du Centre national de la recherche scientifique, p 136
Cotten J, Le Deza A, Baub M, Caroff RC, Maury RC, Dulski P, Fourcade S, Bohn M, Brousse R (1995) Origin of anomalous rare-earth element and yttrium enrichments in subaerially exposed basalts: evidence from French Polynesia. Chem Geol 119:115–138
Denniston RF, González LA, Asmerom Y, Sharma RH, Reagan MK (2000) Speleothem evidence for changes in Indian summer monsoon precipitation over the last ~2300 years. Quat Res 53:196–202
Dettman DL, Reische AK, Lohamann CK (1999) Controls on the stable isotope composition of seasonal growth bands in aragonitic fresh-water bivalve (Unionidae). Geochim Cosmochim Acta 63:1049–1057
Finkel RC, Owen LA, Barnard PL, Cafee MW (2003) Beryllium-10 dating of Mount Everest moraines indicates a strong monsoon influence and glacial synchroneity throughout the Himalaya. Geology 31:561–564
Fralick PW, Kronberg BI (1997) Geochemical distribution of clastic sedimentary rock source. Sediment Geol 113:111–124
France-Lanord C, Derry L, Michard A (1993) Evolution of the Himalaya since Miocene time: isotopic and sedimentologic evidence from the Bengal fan. In: Treloar PJ, Searle M (eds) Himalayan tectonics. Geol Soc Spe Pub, London 74:445–465
Gajurel AP, France-Lanord C, Huyghe P, Guilmette C, Gurung D (2006) C and O Isotope compositions of modern fresh-water mollusc shells and river waters from Himalaya and Ganga plain. Chem Geol 233:156–183
Galy A, France-Lanord C (2001) Higher Erosion rates in the Himalaya: geochemical constraints on riverine fluxes. Geology 29:23–26
Galy A, France-Lanord C, Derry LA (1999) The strontium isotopic budget of Himalayan rivers in Nepal and Bangladesh. Geochim Cosmochim Acta 63:1905–1925
Garzanti E, Vezzoli G, Ando S, France-Lanord C, Singh SK, Foster G (2004) Sand Petrology and focused erosion in collision orogens: the Brahmaputra case. Earth Planet Sci Lett 220:157–174
Garzanti E, Vezzoli G, Ando S, Lavé J, Attal M, France-Lanord C, DeCelles PG (2007) Quantifying sand provenance and erosion (Marsyandi River, Nepal Himalaya. Earth Planet Sci Lett 258:500–515
Garçon M, Chauvel C, France-Lanord C (2013) Sedimentary processes decouple Nd and Hf isotopes in river sediments on continents. Geochim Cosmochim Acta 121:177–195
Gibling MR et al (2005) Discontinuity-bounded alluvial sequences of the southern Gangetic Plains, India: aggradation and degradation in response to monsoonal strength. J Sedim Res 75:369–385
Gourlan A, Meynadier L, Allègre CJ, Tapponnier P, Birck JL, Joron JL (2010) Northern Hemisphere climate control of the Bengali rivers discharge during the past 4 Ma. Quat Res 29:2484–2498
Guillot S, Charlet L (2007) Bengal arsenic, an archive of Himalaya orogeny and paleohydrology. J Environ Sci Health Part A42:1785–1794
Guillot S, Le Fort P (1995) Geochemical constraints on the bimodal origin of high Himalayan leucogranites. Lithos 35:221–234
Guillot S, LeFort P, Pêcher A, Barman MR, Aprahamian J (1995) Contact metamorphism and depth of emplacement of the manaslu granite (Central Nepal). Implications for Himalayan orogenesis. Tectonophysics 241:99–119
Guillot S (1999) An overview of the metamorphic evolution of central Nepal. In: Upreti BN, Le Fort PJ (eds) "Geology of Nepal". J Asian Earth Sci 17:713–725
Gurung JK, Ishiga H, Khadka M (2005) Geological and geochemical examination of arsenic contamination in groundwater in the Holocene Terai Basin, Nepal. Environ Geol 49:98–113
Harper JT, Humphery NF (2003) High altitude Himalayan climate inferred from glacial ice flux. Geophy Res Lett. doi:10.1029/2003GLO17329
Harris N, Inger S (1992) Trace element modelling of pelite-derived granites. Contrib Miner Petrol 110:46–56
Hayashi T, Tanimura Kuwahara Y, Ohno M, Mampuku M, Fujii R, Sakai H, Yamanaka T, Maki T, Uchida M, Yahagi W, Sakai H (2008) Ecological variations in diatom assemblages in the Paleo-Kathmandu Lake linked with global and Indian monsoon climate changes for the last 600,000 years. Quat Res 72:377–387
Huyghe P, Mugnier JL, Gajurel AP, Delcaillau B (2005) Tectonic and climatic control of the changes in the sedimentary record of the Karnali River section (Siwaliks of western Nepal). Isl Arcs 14:311–325. doi:10.1111/j.1440-1738.2005.00500.x
Ishiga H, Dozen K, Yamazaki CFA, Islam MB, Rohman MH, Sattar MA, Yamamoto H, Itoh K (2000) Geological constraints on arsenic contamination of groundwater in Bangladesh. In: Proceedings of the 5th forum of Arsenic in Asia, Nov 2000 Asia Arsenic Network (AAN), Yokohama Japan, pp 53–62
Kaufman DS, Ager TA, Anderson NJ, Anderson PM, Andrews JT, Bartlein PJ, Brubaker LB, Coats LL, Cwynar LC, Duvall ML, Dyke A, Edwards ME, Eisner WR, Gajewski K, Geirsdottir A, Hu FS, Jennings AE, Kaplan, Kerwin MW, Lozhkin AV, MacDonald GM, Miller GH, Mock CJ, Oswald WW, Otto-Bliesner BL, Porinchu DF, Ruhland K, Mol JP, Steig EJ, Wolfe BB (2004) Holocene thermal maximum in the western Arctic 0–180 W. Quat Sci Rev 23:529–560. doi:10.1016/j.quascirev.2003.09.007
Lavé J, Avouac JP (2001) Fluvial incision and tectonic uplift across the Himalayas of central Nepal. J Geophy Res 106:26561–26591. doi:10.1029/2001JB000359
Lupker M, France-Lanord C, Galy V, Lavé J, Gaillardet J, Gajurel AP, Guilmette C, Rahman M, Singh SK, Sinha R (2012) Predominant floodplain over mountain weathering of Himalayan sediments Ganga basin. Geochim Cosmochim Acta 84:410–432
Lécuyer C, Reynard B, Martineau F (2004) Stable isotope fractionation between mollusc shells and marine waters from Martinique Island. Chem Geol 213:293–305
McArthur JM, Ravenscroft P, Safiullah S, Thirlwall MF (2001) Arsenic in groundwater: testing pollution mechanism for sedimentary aquifers in Bangladesh. Water Res Res 37:109–117
McCrea JM (1950) On the isotopic chemistry of carbonates and a paleotemperature scale. J Chem Phys 18:849–857
McDonough W, Sun SS (1995) The composition of the earth. Chem Geol 120:223–253
McLennan SM, Hemming S, McDennial DK, Hanson GN (1993) Geochemical approaches to sedimentation provenance and tectonics. Geol Soc Amer Bull 284:21–40
Meharg AA, Scrimgeour C, Hossain SA, Fuller K, Cruickshank K, Williams PN, Kinniburgh DG (2006) Codeposition of organic carbon and arsenic in Bengal delta aquifers. Environ Sci Technol 40:4928–4935
Milliman JD, Sivitsli JPM (1992) Geomorphic/tectonic control of sediment discharge to the ocean: the importance of small mountainous rivers. J Geol 100:525–544

Mugnier JL, Leturmy P, Huyghe P, Chalaron E (1999) The Siwaliks of Western Nepal: mechanism of the Thrust Wedge. In: Le Fort P, Upreti BN (eds) Geology of the Nepal Himalaya: recent advances. J Asia Earth Sci 17:643–657

Nesbitt HW, Fedo CM, Young GM (1997) Quartz and feldspar stability, steady and non-steady-state weathering and petrogenesis of siliclastic sands and muds. J Geol 105:173–191

Nath B, Chakraborty S, Burnol A, Stüben D, Chatterjee D, Charlet L (2009) Mobility of arsenic in the subsurface environment: an integrated hydrogeochemical study and sorption model of the sandy aquifer materials. J Hydrol 364:236–248

Paudel LP (2012) Carbonaceous schists of the Main Central Thrust zone as a source of graphite: a case study from the Kali Gandaki valley, west Nepal. Bull Dept Geol Tribhuvan Univ Kathmandu Nepal 14:9–14

Plant JA, Kinniburgh DG, Smedley PL, Fordyce FM, Klinck BA (2003) Arsenic and selenium. Treatise on geochemistry. In: Lollar BS, Heinrich D. Holland, Karl K (eds) Turekian9. doi:10.1016/B0-08-043751-6/09047-2:17-66

Pokhrel D, Bhandari BS, Viraraghavan T (2009) Arsenic contamination of groundwater in the Terai region of Nepal: an overview of healths concerns and treatment options. Environ Geol 35:157–161

Potter PE, Maynard JB, Depteris P (2005) Mud and mudstones, introduction and overview. Springer-verlag, Berlin, p 218

Rashid SA (2002) Geochemical characteristics of Mesoproterozoic clastic sedimentary rocks from the Chakrata Formation, Lesser Himalaya; implications for crustal evolution and weathering history in the Himalaya. J Asian Earth Sci 21:283–293

Reddy KR, DeLaune RD (2008) Biogeochemistry of wetlands: science and applications. Taylor and Francis group, London 774

Reichart GJ, Lourens LJ, Zachariasse WJ (1998) Temporal variability in the northern Arabian Sea Oxygen Minimum Zone OMZ during the last 225,000 years. Paleoceanography 13:607–621

Shah BA (2008) Role of Quaternary stratigraphy on arsenic-contaminated groundwater from parts of Middle Ganga Plain, UP-Bihar, India. Environ Geol 53:1553–1561

Sharma S, Joachimski M, Sharma ML, Tobschal HJ, Singh IB, Sharma C, Chaulan MS, Morgenroth G (2004) Late glacial and Holocene environmental changes in Ganga plain, Northern India. Quat Sci Rev 23:145–159

Shukla U, Bora K (2009) Sedimentation model of gravel-dominated alluvial piedmont fan, Ganga Plain, India. Int Earth Sci 98:443–459

Singh P (2009) Major, trace and REE geochemistry of the Ganga River sediments: influence of provenance and sedimentary process. Chem Geol 266:2516264

Sinha R, Friend KH (1994) River systems and their flux, Indo-Gangetic plains, Norther Bihar, India. Sedimentology 41:825–845

Smedley PL, Kinniburgh DG (2002) A review of the source, behaviour and distribution of arsenic in natural waters. Appl Geochem 17:517–568

Tardy Y, Nahon D (1985) Geochemistry of laterites, stability of Al-goethite, Al-hematite, and Fe3+ -kaolinite in bauxites and ferricretes: an approach to the mechanism of concretion formation. Am J Sci 285:865–903

Taylor SR, McLennan SM (1985) The continental crust: its composition and evolution. Oxford Blackwell, London 312

Tripathi JK, Ghazanfari P, Rajamani V, Tandon SK (2007) Geochemistry of sediments of the Ganges alluvial plains: evidence of large-scale sediment recycling. Quat Int 159:119–130

Tsukamoto S, Asahi K, Watanabe T, Rink WJ (2002) Timing of past glaciations in Kanchenjunga Himal, Nepal by optically stimulated luminescence dating of tills. Quat Int 97–98:57–67

Tzedakis PC, Andrieu V, De Beaulieu JL, de Crowhurst S, Follieri M, Hooghiemstra H, Magri D, Reille M, Sadori L, Shackleton NJ, Wijmstra TA (1997) Comparison of terrestrial and marine records of changing climate of the last 500,000 years. Earth Planet Sci Lett 150:171–176

UNDP and Nepal HMGO (1989) Shallow groundwater investigation in Terai, Nawalparasi district West. Technical report 5 p 21

Upreti BN (1999) An overview of the stratigraphy and tectonics of the Nepal Himalaya. J Asian Earth Sci 17:577–606

van Geen A, Radloff K, Aziz Z, Cheng Z, Huq MR, Ahmed KM, Weinman B, Goodbred S, Jung HB, Zheng Y, Berg M, Trang PTK, Charlet L, Metral J, Tisserand D, Guillot S, Chakraborty P, Gajurel AP, Upreti BN (2008) Comparison of arsenic concentrations in simultaneously-collected groundwater and aquifer particles from Bangladesh, India, Vietnam, and Nepal. Appl Geochem 23:3244–3251

Zhao M, Beveridge NAS, Shackleton NJ, Sarnthein M, Eglinton G (1995) Sediment core ODP 658, interpreted sea surface temperature, Eastern Tropical Atlantic. Paleoceanography 10:661–675. doi:10.1029/94PA03354